Brain, Behavior, & Immunity - Health 52 (2026) 101187

Contents lists available at ScienceDirect

Brain, Behavior, & Immunity - Health

journal homepage: www.editorialmanager.com/bbih/default.aspx

# Immunoglobulin G complexes from post-infectious ME/CFS, including post-COVID ME/CFS disrupt cellular energetics and alter inflammatory marker secretion☆

Zheng Liu [a], Claudia Hollmann [a], Sharada Kalanidhi [b], Stephanie Lamer [c], Andreas Schlosser [c], Emils Edgars Basens [d], Georgy Nikolayshvili [d], Liba Sokolovska [d], Gabriela Riemekasten [e], Rebekka Rust [f,g], Judith Bellmann-Strobl [f,g], Friedemann Paul [f,g], Robert K. Naviaux [h], Zaiga Nora-Krukle [d], Franziska Sotzny [i], Carmen Scheibenbogen [i], Bhupesh K. Prusty [a,d,*]

[a] Institute of Virology and Immunobiology, University of Würzburg, Germany
[b] Stanford Genome Technology Center, Stanford University School of Medicine, Stanford, CA, USA
[c] Rudolf Virchow Center, Center for Translational Bioimaging, Julius-Maximilians-University of Würzburg, Germany
[d] Institute of Microbiology and Virology, Riga Stradiņš University Research Center, Riga, Latvia
[e] Klinik für Rheumatologie, Universitätsklinikum Schleswig-Holstein, Lübeck, Germany
[f] Experimental and Research Center (ECRC), Charité - Universitätsmedizin Berlin, Corporate Member of Freie Universität Berlin, Humboldt Universität zu Berlin and Berlin Institute of Health, Berlin, Germany
[g] NeuroCure Research Centre, Charité - Universitätsmedizin Berlin, Corporate Member of Freie Universität Berlin, Humboldt Universität zu Berlin and Berlin Institute of Health, Berlin, Germany
[h] Departments of Medicine, Pediatrics, and Pathology, University of California, San Diego School of Medicine, San Diego, USA
[i] Institute of Medical Immunology, Charité – Universitätsmedizin Berlin, Corporate Member of Freie Universität Berlin and Humboldt Universität zu Berlin and Berlin Institute of Health, Berlin, Germany

ARTICLE INFO

*Keywords:*
Immunoglobulin
Antigen
Antibody
Mitochondria
Post-viral chronic illnesses
ME/CFS
Post COVID

ABSTRACT

*Background:* Autoimmunity is a key clinical feature in both post-infectious Myalgic encephalomyelitis/chronic fatigue syndrome (ME/CFS) and Post-Acute Sequelae of COVID (PASC). Passive transfer of immunoglobulins from patients' sera into mice induces some clinical features of PASC. However, the physiological effects of immunoglobulins on cellular alterations remain elusive. In this study, we tested the potential effects of immunoglobulins from ME/CFS patients on endothelial cell dysfunction.

*Methods:* We have isolated immunoglobulins from 106 individuals, including ME/CFS (n = 39), PCS-CFS (n = 15), MS (n = 20) patients, and healthy controls (n = 41). Protein composition of the isolated immune complexes was studied using mass spectrometry. The effect of isolated immune complexes on mitochondria was evaluated using confocal microscopy and a Seahorse XFe96 Extracellular Flux Analyzer, and the impact on inflammatory cytokine secretion was studied using a multiplex bead-based assay.

*Results:* Here, we demonstrate that IgG isolated from post-infectious ME/CFS patients selectively induces mitochondrial fragmentation in human endothelial cells and alters cellular energetics. This effect is lost upon cleavage of IgG into its Fab and Fc fragments. The digested Fab fragment from ME/CFS alone was able to alter the cellular energetics, resembling the effect of intact IgG. IgG from post-infectious ME/CFS, including post-COVID ME/CFS patients, induced distinct but separate cytokine secretion profiles in healthy PBMCs. Proteomics analysis of IgG-bound immune complexes revealed significant changes in immune complexes from ME/CFS patients, affecting extracellular matrix organization, whereas those from post-COVID ME/CFS patients pointed to alterations in hemostasis and blood clot regulation.

*Conclusions:* We demonstrate that IgGs from ME/CFS patients carry a chronic protective stress response that promotes mitochondrial adaptation via fragmentation, without altering mitochondrial ATP generation capacity

☆ **One Sentence Summary:** IgG immune complexes from ME/CFS patients differ from those of healthy individuals and affect mitochondrial structure and energetics.

* Corresponding author. Institute of Virology and Immunobiology, University of Würzburg, Germany.
*E-mail address:* bhupesh.prusty@rsu.lv (B.K. Prusty).

https://doi.org/10.1016/j.bbih.2026.101187
Received 23 January 2026; Accepted 25 January 2026
Available online 4 February 2026

in endothelial cells. Together, these results highlight a potential pathogenic role of IgG in post-infectious ME/CFS and point to novel therapeutic strategies targeting antibody-mediated metabolic dysregulation.

## 1. Background

Myalgic Encephalomyelitis/Chronic Fatigue Syndrome (ME/CFS) is a complex, debilitating, chronic, long-term illness that involves immune dysfunction, autonomic nervous system dysfunction, and metabolic alterations (Myhill et al., 2009; Mandarano et al., 2020; Zinn and Jason, 2021). Key symptoms of ME/CFS include fatigue, which can be both mental and physical in nature, such as post-exertional malaise (PEM) (Brown and Jason, 2020), cognitive dysfunction ("brain fog"), etc (Cvejic et al., 2016).

Emerging evidence implicates endothelial cell dysfunction as a key contributor to the chronicity of ME/CFS. Recent studies have observed reduced macro- and microvascular endothelial function in ME/CFS patients compared to matched controls, suggesting impaired vasodilation and compromised vascular homeostasis (Sandvik et al., 2023; Haffke et al., 2022). Endothelial cells, by virtue of their role in regulating blood flow, nutrient and oxygen delivery, and leukocyte trafficking, become central in this pathology. Endothelial cell dysfunction can provide a unifying explanation for both physical and mental fatigue in ME/CFS and its persistence over time. Endothelial dysfunction can lead to a combination of vascular, metabolic, and neuro-immune perturbations that create a self-reinforcing feedback loop, locking patients into a state of chronic, disproportionate fatigue and worsening post-exertional symptoms. *In vitro* experiments showed that endothelial cells exposed to plasma from ME/CFS patients secreted less nitric oxide (NO) and exhibited reduced eNOS activity, linking circulating factors to impaired endothelial responsiveness (Bertinat et al., 2022).

ME/CFS patients frequently exhibit altered regulation of the autonomic and immune systems (Sotzny et al., 2018). In recent years, several studies have focused on the role of autoimmunity in ME/CFS, showing elevated levels of antibodies targeting β2 adrenergic receptors (β2 AdR) and muscarinic M3 and M4 acetylcholine receptors in subsets of ME/CFS patients (Bynke et al., 2020; Loebel et al., 2016; Scheibenbogen et al., 2018; Hartwig et al., 2020). The correlation of these autoantibodies with clinical symptoms suggests their functional role in ME/CFS (Sotzny et al., 2022). Two recent studies reported the induction of ME/CFS and long COVID-like symptoms in mice following the passive transfer of IgG from patients (Chen et al., 2024; Santos Guedes de Sa et al., 2024). These findings collectively highlight the potential role of autoantibodies in the pathophysiology of ME/CFS, particularly in disrupting the regulation of autonomic and immune systems. In this study, we investigated the potential role of circulating human IgGs in mitochondrial, cellular, and immunological alterations *in vitro*.

## 2. Results

### 2.1. Passive transfer of IgGs from ME/CFS patients induces mitochondrial fragmentation

Mitochondrial alterations are among the most powerful drivers of endothelial cell dysfunction because endothelial cells rely heavily on tightly regulated mitochondrial signaling, not primarily for ATP production, but for redox balance, nitric oxide (NO) signaling, calcium handling, and inflammatory control. When mitochondrial homeostasis is disrupted, multiple endothelial pathways essential for vascular health collapse simultaneously. Immune dysregulation is closely associated with mitochondrial dysfunction, which is a characteristic feature of ME/CFS. Several groups, including ours, have previously shown that serum-derived unknown factors from ME/CFS patients can induce mitochondrial alterations in healthy cells (Schreiner et al., 2020; Fluge et al., 2016; Esfandyarpour et al., 2019). A lack of complement activation and pathogen clearance can allow several opportunistic pathogens to replicate, resulting in the production of a wide array of IgG and IgM autoantibodies in the serum. We hypothesized that some of the altered antibodies in serum or altered antigen-antibody complexes might induce chronic mitochondrial dysfunction. To investigate this *in vitro*, we purified IgGs (Fig. 1A) from human serum and exposed them to two independent cell types, primary human foreskin fibroblasts (HFFs) and primary human umbilical vein endothelial cells (HUVECs), and followed their entry into the cells using immunoblotting (Fig. 1B). HUVECs were permissive to human IgG, while HFFs did not allow entry of IgG into the cells (Fig. 1C), suggesting cell-specific selective entry of IgG into human cells. IgG entry into HUVEC cells was also confirmed using immunofluorescence staining of human IgG (Fig. 1D). IgG that entered HUVEC cells was efficiently detectable up to 16 h post-exposure (Fig. 1E). However, IgG levels decreased within the cells in a time-dependent manner (Fig. 1E), suggesting potential IgG recycling and degradation within the cell. Fc-specific fragments (~35 kDa) of IgG remained abundantly detectable within the cells till 48 h post-exposure (Fig. 1E). No significant differences in IgG entry and survival of Fc-specific IgG fragments were observed between different disease groups (Fig. 1F).

Exposure to as low as 1 μg/ml of IgGs from ME/CFS and PCS-CFS patients significantly fragmented mitochondria in HUVECs within 16 h of exposure, as assessed by confocal imaging (Fig. 2A) and subsequent quantification of average mitochondrial surface area (Fig. 2B). Although the statistical significance for changes in average mitochondrial surface area was strong for the ME/CFS cohort (HD vs. ME/CFS, $P = 0.0004$), IgG-induced alterations in mitochondrial surface area were not distinct in the entire ME/CFS cohort. Only a subgroup of patients induced significant mitochondrial fragmentation. Hence, we conducted a gender-based analysis, which revealed substantial IgG-induced mitochondrial fragmentation in female ME/CFS and PCS-CFS patients compared with male patients (Fig. 2C). IgG-induced mitochondrial fragmentation was also not observed when cells were exposed to IgGs from patients with multiple sclerosis (Fig. 2B–C). Multiple linear regression analysis involving disease severity (as measured by Bell score), gender, and average mitochondrial surface area did not show any significant associations in ME/CFS and PCS-CFS (Supplementary Fig. S1; see Supplementary methods for more details). However, disease severity was significantly predictive of average mitochondrial surface area in MS patients.

Drp1 protein play a key role in mitochondrial fragmentation and its functional significance in mitochondrial quality control (Wang et al., 2025). Hence, we tested if IgG-induced mitochondrial fragmentation is Drp1-dependent. IgG from ME/CFS and PCS-CFS patients decreased the protein levels of Drp1, mitofilin, Miga1, and PLD6 (Fig. 2D and E). Interestingly, the levels of the mitophagy marker protein LC3β showed a trend toward decreased levels in the presence of IgG from ME/CFS and PCS-CSF patients (Fig. 2D and E), but this difference was not statistically significant. Blocking the Fc receptors on the HUVEC cell surface did not completely prevent IgG entry into cells (Fig. 2F). Higher concentrations of the Fc blocker resulted in decreased IgG entry (Fig. 2F). However, there was significant cell loss at that concentration, as evident from a decrease in Drp1, p53, Tom20, and Vinculin protein levels. To understand the mechanism of IgG entry into cells, we digested IgG and separated both Fab and Fc fragments (Fig. 2G). Both fragments were able to enter the cell with equal efficiency (Fig. 2H). However, separated Fab and Fc fragments did not induce a fragmented mitochondrial phenotype (Fig. 2I) with the same efficiency as their IgG counterpart. These results suggest that intact IgG from ME/CFS patients induces mitochondrial fragmentation, which might be independent of the classical Drp1-induced pathways.

### 2.2. IgGs from ME/CFS patients alter cellular energetics

We then asked if IgG-induced changes in mitochondrial architecture also alter mitochondrial energetics. To assess the functional changes in the cellular energetics profile, we performed mitochondrial stress tests using the Seahorse XFe96 Extracellular Flux Analyzer. Following 36 h IgG exposure, HUVECs were analyzed for changes in oxygen consumption rate (OCR) and extracellular acidification rate (ECAR). Sequential injections of oligomycin, FCCP, and rotenone/antimycin A allowed for assessment of mitochondrial respiration parameters. Given the pronounced and well-documented interplate variability in the seahorse assay, as evident in our data and others (Yepez et al., 2018; Mercier-Letondal et al., 2021), we conducted our assays in two separate groups. Each group included IgG from ME/CFS patients, either with a strong mitochondrial fragmentation phenotype or without it. On each assay plate, we tested 10 healthy controls, 10 ME/CFS patients, and either 10 PCS-CFS patients or 10 MS patients. IgG from healthy controls, PCS-CFS, and MS patients induced similar OCR patterns in HUVECs, while HUVECs exposed to IgG from ME/CFS patients with mitochondrial fragmentation phenotype exhibited a trend towards higher basal respiration (not statistically significant) and significantly increased (Fig. 3A) spared respiration capacity. However, this phenomenon was not detected with IgG from ME/CFS patients without a mitochondrial fragmentation phenotype (Supplementary Fig. S2A). This suggests that

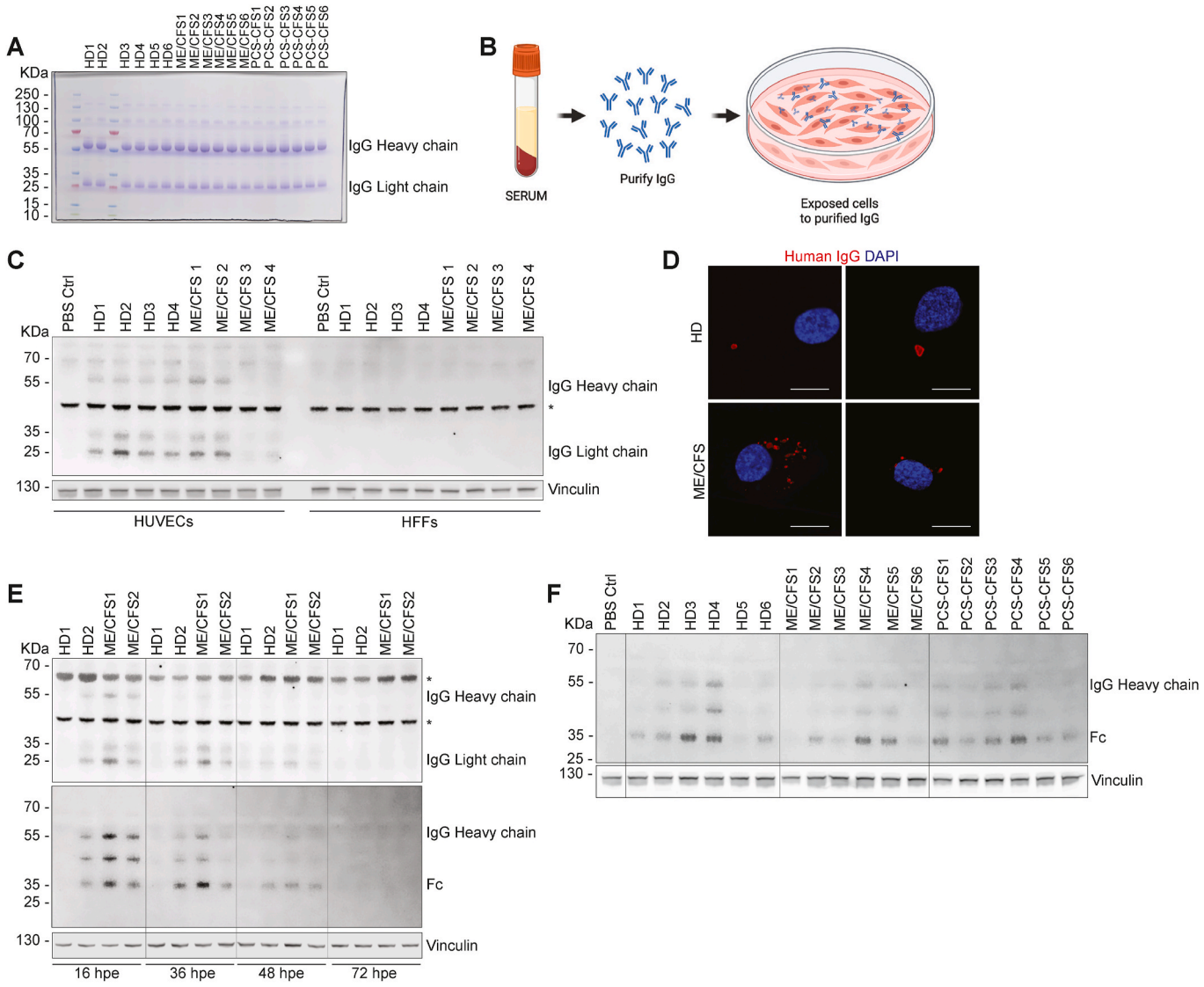


**Fig. 1. Selective entry of IgG into human cells and its turnover.**

A. The quality and quantity of purified IgG were assessed by running them on denaturing SDS-PAGE gels and staining with Coomassie.

B. Schematics of IgG entry assay.

C. Immunoblot analysis reveals the presence of intracellular IgG heavy and light chains in HUVECs, but not in HFFs, following exposure to 1 μg/mL purified IgG from ME/CFS patients or control sera for 12 h. Vinculin was used as a loading control.

D. Confocal microscopy images show intracellular human IgG in primary HUVECs exposed to 1 μg/mL purified IgG from patient and control sera. Two representative images are shown for each condition.

E. Immunoblot analysis reveals degradation of intracellular IgG heavy and light chains in HUVECs at 16, 36, 48, and 72 h following exposure to 1 μg/mL purified IgG from ME/CFS patients or control sera. Vinculin was used as a loading control. Fc-specific secondary antibody was used (middle panel) to detect the full-length heavy chain of IgG and cleaved Fc fragments.

F. Immunoblot analysis comparing intracellular IgG heavy and Fc-specific fragments in HUVECs at 16 h following exposure to 1 μg/mL purified IgG from HD, ME/CFS, and PCS-CFS patient sera. Vinculin was used as a loading control. Fc-specific secondary antibody was used to detect the full-length heavy chain of IgG and cleaved Fc fragments.

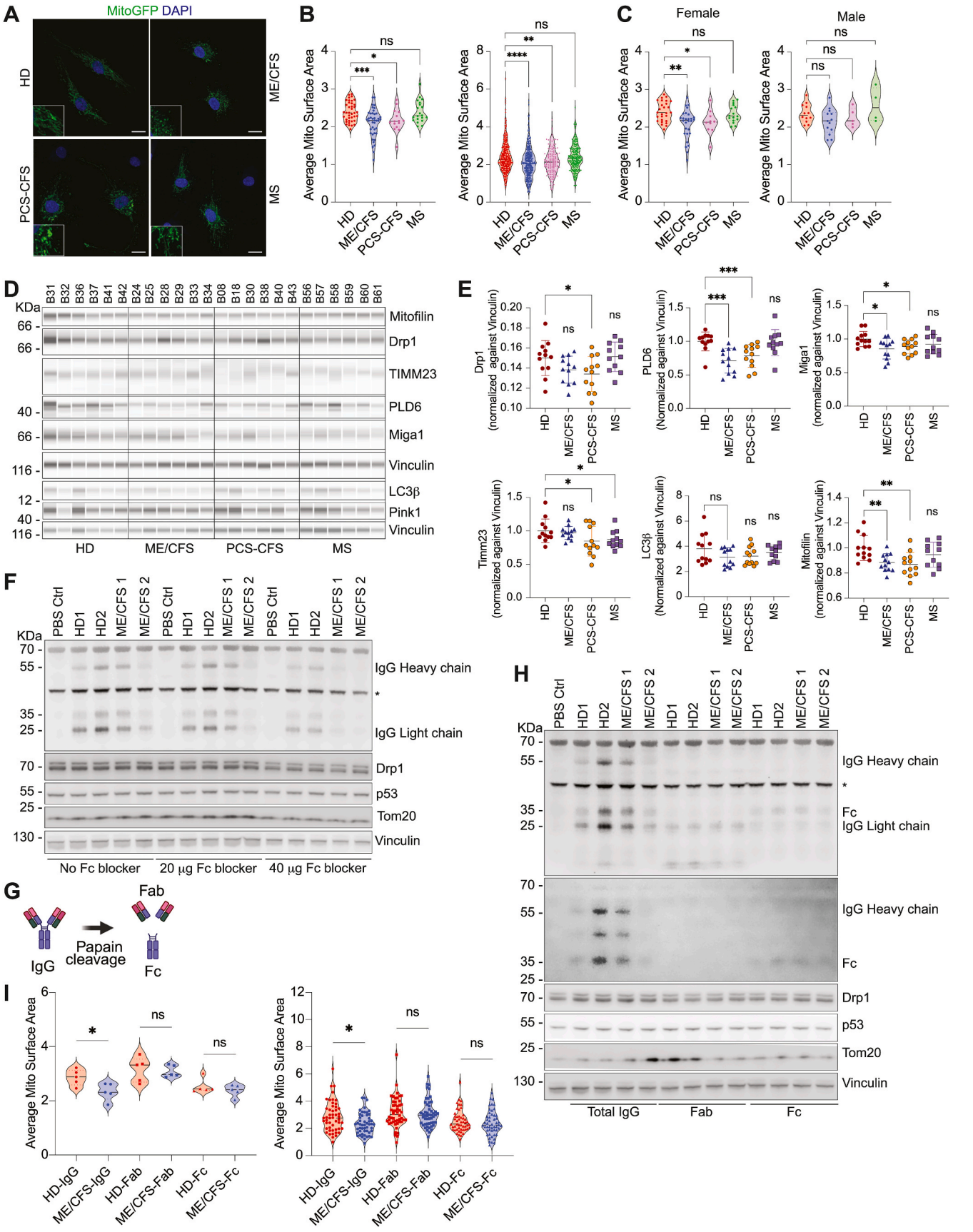


*(caption on next page)*

**Fig. 2. IgG from ME/CFS patients induces mitochondrial fragmentation.**

A. Representative confocal microscopy images show mitochondrial architecture in primary HUVECs expressing stable GFP within mitochondria and exposed to 1 μg/mL purified IgG from ME/CFS, PCS-CFS, and MS patient and control sera. One representative image is shown for each condition.

B. Quantification of average mitochondrial surface area in primary HUVECs exposed to 1 μg/mL purified IgG from ME/CFS (n = 39), PCS-CFS (n = 15), MS (n = 20) patients, and healthy controls (n = 41). At least 10 cells were imaged per sample, derived from 3 replicates. In the left panel, each point represents the mean surface area across all images for each subject. In the right panel, each point represents the surface area measured from a single image. Two-tailed Mann-Whitney *U* test. (Left) HD vs ME/CFS, ***P = 0.0004. HD vs PCS-CFS, *P = 0.0164. HD vs MS, ns P = 0.8676. (Right) HD vs ME/CFS, ****P < 0.0001. HD vs PCS-CFS, **P = 0.0067. HD vs MS, ns P = 0.4794.

C. Gender-based separation of average mitochondrial surface area from the above experiment. Each point represents the surface area measured from a single image. Two-tailed Mann-Whitney *U* test. (Female) HD vs ME/CFS, **P = 0.0018. HD vs PCS-CFS, *P = 0.0173. HD vs MS, ns P = 0.4938. (Male) HD vs ME/CFS, ns P = 0.0976. HD vs PCS-CFS, ns P = 0.5058. HD vs MS, ns P = 0.4462.

D. Capillary-based automated Immunoblot analysis of Mitofilin, Drp1, TIMM23, PLD6, Miga1, LC3β, Pink1 protein levels in HUVEC cells 36 h after exposure to 1 μg/mL of purified IgG from ME/CFS (n = 12), PCS-CFS (n = 12), and MS (n = 11) patient and control (n = 12) sera. Vinculin was used as a loading control.

E. Fold change values from the above immunoblot analysis were derived from densitometric analysis of bands, normalized to the same value for vinculin. Two-tailed Mann-Whitney *U* test. (Drp1) HD vs ME/CFS, ns P = 0.0684. HD vs PCS-CFS, *P = 0.0387. HD vs MS, ns P = 0.7859. (PLD6) HD vs ME/CFS, ****P < 0.0001. HD vs PCS-CFS, ***P = 0.0007. HD vs MS, ns P = 0.6075. (Timm23) HD vs ME/CFS, ns P = 0.1402. HD vs PCS-CFS, *P = 0.0317. HD vs MS, *P = 0.0106. (Miga1) HD vs ME/CFS, *P = 0.0284. HD vs PCS-CFS, *P = 0.0449. HD vs MS, ns P = 0.1896. (LC3β) HD vs ME/CFS, ns P = 0.0684. HD vs PCS-CFS, ns P = 0.1600. HD vs MS, ns P = 0.6075. (Mitofilin) HD vs ME/CFS, **P = 0.0056. HD vs PCS-CFS, **P = 0.0029. HD vs MS, ns P = 0.3164.

F. Immunoblot analysis shows a decreased amount of intracellular IgG heavy and light chains in HUVECs pretreated with Fc blocker before the exposure to 1 μg/mL purified IgG from ME/CFS patients or control sera for 12 h. Vinculin was used as a loading control.

G. Schematics of IgG cleavage assay.

H. Immunoblot analysis shows the presence of intracellular IgG heavy and light chains in HUVECs after exposure to 1 μg/mL purified IgG, purified Fab fragments, and Fc fragments from ME/CFS patients or control sera for 12 h. Vinculin was used as a loading control. Fc-specific secondary antibody was used (second panel) to detect the full-length heavy chain of IgG and cleaved Fc fragments.

I. Quantification of average mitochondrial surface area in primary HUVECs exposed to 1 μg/mL purified IgG or Fab Fragment or Fc fragment from 5 ME/CFS, and 5 controls. In the upper panel, each point represents the mean surface area across all images for each individual. In the lower panel, each point represents the surface area measured from a single image. Two-tailed Mann-Whitney *U* test. (Upper Panel) HD vs ME/CFS IgG, *P = 0.0317. HD vs ME/CFS Fab, ns P = 0.8413. HD vs ME/CFS Fc, ns P = 0.6905. (Lower Panel) HD vs ME/CFS IgG, *P = 0.0130. HD vs ME/CFS Fab, ns P = 0.5572. HD vs ME/CFS Fc, ns P = 0.3662. (For interpretation of the references to colour in this figure legend, the reader is referred to the Web version of this article.)

IgG-induced mitochondrial fragmentation is directly associated with increased spared respiration capacity. In the meantime, ECAR, which indicates glycolytic activity, showed no differences in patterns. Baseline ECAR levels were comparable among all four patient groups (Fig. 3B, Supplementary Fig. S2B). ATP measurement assays did not reveal any significant changes in glycolytic, mitochondrial, or total ATP levels in response to IgG treatment (Supplementary Fig. S2C–S2H).

To force the cells to rely exclusively on oxidative phosphorylation (OXPHOS), we replaced glucose-containing culture media with galactose-containing media, thereby isolating mitochondrial function from glycolysis. Due to the substitution with galactose, the cells had already reached their maximum respiratory capacity at baseline (Fig. 3C). In contrast to cells cultured in glucose-containing media, HUVECs exposed to IgGs from the three study groups did not exhibit differences in OCR or ECAR patterns (Fig. 3D). These results showed that the ME/CFS IgG-induced increase in maximal respiratory capacity of cells is possibly not compensated by mitochondrial oxidative phosphorylation alone, and the observed effect is masked when cells are forced to rely solely on OXPHOS.

We then compared the potential effects of separated Fab and Fc fragments on cellular energetics to those of the intact IgGs. Fab fragments of IgG mimicked the intact IgG effects of ME/CFS patients (Fig. 4A), indicating their predominant role in increasing the respiration of HUVECs induced by IgGs from ME/CFS. On the contrary, Fc fragments from healthy controls induced an overall metabolic rate of respiration in HUVECs. This was also reflected in total, glycolytic, as well as mitochondrial ATP levels of HUVECs in the presence of Fc fragment from healthy controls (Fig. 4B). However, due to large variations in ATP counts across the 5 healthy controls, we could not detect a statistically significant difference in ATP levels in these studies (Fig. 4B). Taken together, our results suggest that IgG-induced alterations in mitochondrial morphology and energetics are potentially two independent phenotypes.

### *2.3. IgGs from ME/CFS patients induce secretion of specific inflammatory cytokines*

Mitochondria play a significant role beyond energetics. Alterations in mitochondrial structure and function can release various mitochondrial components and metabolic products that can function as damage-associated molecular patterns (DAMPs) and promote inflammation when released into the cytosol (Marchi et al., 2023). Alternatively, direct interaction of IgG-TLR complexed ligands can induce pro-inflammatory cytokines (Vogelpoel et al., 2014). Therefore, we tested whether passive transfer of IgG to healthy PBMCs can trigger inflammatory markers often associated with the ME/CFS (Fig. 5A). Ten well-known cytokines were measured in a multiplexed bead-based assay. The same IgGs were exposed to two separate PBMC samples from independent healthy donors, and two independent biological replicates were carried out for each IgG treatment. IgGs from a large subset of ME/CFS patients induced the secretion of four cytokines, including IL-1β (P = 0.0460, IFNγ (P = 0.0675), TNFα (P = 0.1653) and IL-6 (P = 0.0675), (Fig. 5B). However, this inflammatory cytokine induction phenotype was not uniform for all ME/CFS patients, making the differences statistically insignificant (Fig. 5B) except for IL-1β. Notably, 48 h exposure of PBMCs to IgG from MS patients significantly induced the levels of 3 cytokines, including IL-5, IL-10, and TNFβ, and reduced levels of TGFα (Fig. 5B). A similar trend was also observed when PBMCs were treated with IgG from PCS-CFS patients. However, IgGs from ME/CFS patients had no effect on the secretion of these cytokines. Levels of IFNα2 were not altered by IgG from all 4 study groups. We verified alterations in some of these cytokines using alternative ELISA-based commercial assays (Supplementary Fig. S3A) that mostly replicated the multiplex assay results. In these studies, IgGs from ME/CFS patients exhibited a contrasting phenotype compared with those from PCS-CFS patients. In summary, these results demonstrated that patient IgG can induce the secretion of specific inflammatory cytokines; however, they could not establish a direct causal link between IgG-induced mitochondrial fragmentation and inflammation, suggesting a role for a mitochondria-independent pathway.

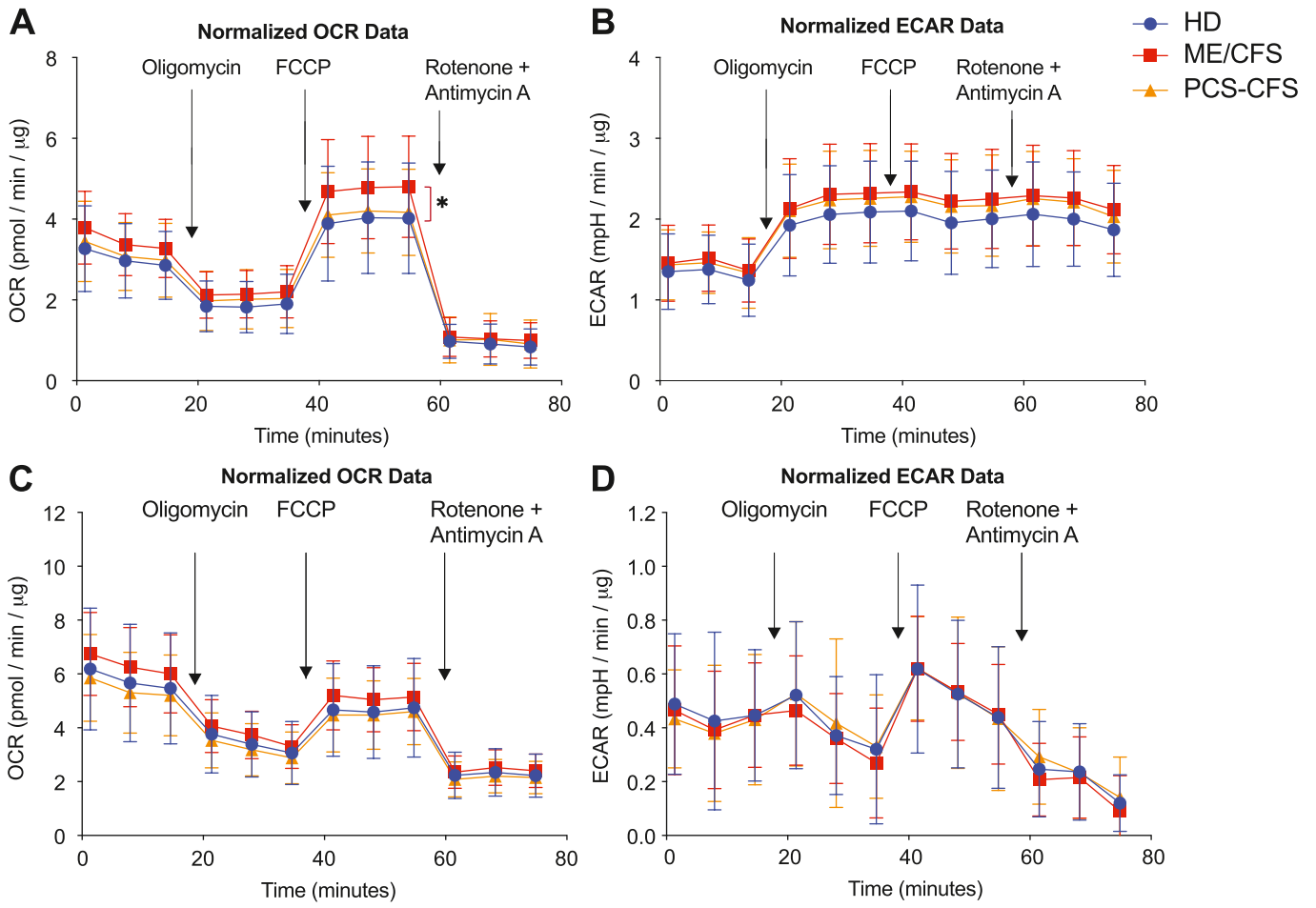


**Fig. 3. ME/CFS IgGs alter metabolic energetics in HUVECs.**
(A-D) Cellular energetics profiles from Seahorse XF Cell Mito Stress Test are shown from HUVECs exposed to 1 µg/mL IgGs from healthy control (HD) (n = 10), ME/CFS (n = 10), PCS-CFS (n = 10) patients. Normalized OCR (A, C) and normalized ECAR (B, D) are shown.
For A-B, HUVECs were grown in medium containing glucose and for C-D, cells were grown in galactose containing media.
Each patient IgG was exposed to independent cells in three separate wells on each assay plate. Additionally, the same assay was performed at least three times on three separate days, and one representative result is shown here.

### *2.4. Autoantibodies as a potential cause of mitochondrial fragmentation*

IgG-induced mitochondrial fragmentation can be caused by specific autoantibodies enriched in ME/CFS and PCS-CFS patients. Numerous publications have shown that one or more autoantibodies are elevated in ME/CFS patients, making it challenging to correlate a specific autoantibody with the mitochondrial phenotype. We conducted a proof-of-concept pilot study utilizing commercial protein microarrays. To test potential IgG and IgM responses to selective autoantigens frequently involved in autoimmune diseases, we measured IgG and IgM levels against 120 autoantigens (Supplementary Table 2) in a small cohort of mild-to-severe ME/CFS patients (n = 12) and healthy controls (n = 3). Samples were blinded throughout the experimental procedure and data analysis. Multivariate clustering of log-transformed data revealed that patients could be separated into distinct groups, comprising healthy, mild/moderate, and severe patients (Fig. 5C), based on IgM antibody levels against antigens such as PCNA, collagen V and VI, complement C3, and CRP (Fig. 5D–F). IgM against fibronectin was negatively associated with disease severity. A similar analysis of IgG levels against autoantigens failed to differentiate cases from controls (Supplementary Fig. S3B). One major limitation of our current approach, Sepharose G bead-based IgG purification, is that it does not purify the majority of natural IgM, which are pentameric structures, making it challenging to correlate IgM autoantibody levels to mitochondrial fragmentation. While these results suggest that IgM levels against known autoantigens can distinguish between ME/CFS disease groups and healthy individuals, they may not be responsible for mitochondrial fragmentation.

### *2.5. Proteomic analysis of immune complexes*

Immunoglobulin-mediated alterations in cellular energetics could be transmitted via antigen-antibody complexes. ME/CFS is closely associated with immune dysregulation, yet no definitive biomarkers have been identified. Plasma proteomic analysis has been shown to be a powerful tool to identify biomarkers in certain diseases (Ward et al., 2024; Geyer et al., 2017), including ME/CFS (Germain et al., 2021; Milivojevic et al., 2020). Purified IgG from human serum mainly contains immunoglobulin fractions with freely available Fc receptors along with associated immune complex proteins. Unlike plasma proteomics, which analyzes all circulating proteins, immune complex proteomics enriches for antibody-bound proteins, making it specific for identifying immune complex-related proteins and disease-specific immune functions, such as those associated with autoimmune diseases. To identify fine changes within the immune complex compositions, we carried out mass spectrometry analysis of purified immunoglobulin fractions from ME/CFS (n = 40), PCS-CFS (n = 16), healthy controls (n = 39), and multiple sclerosis (n = 11) (Fig. 6A). Our analysis did not detect any EBV or HHV-6A protein signature within the immune complex proteome. Based on the

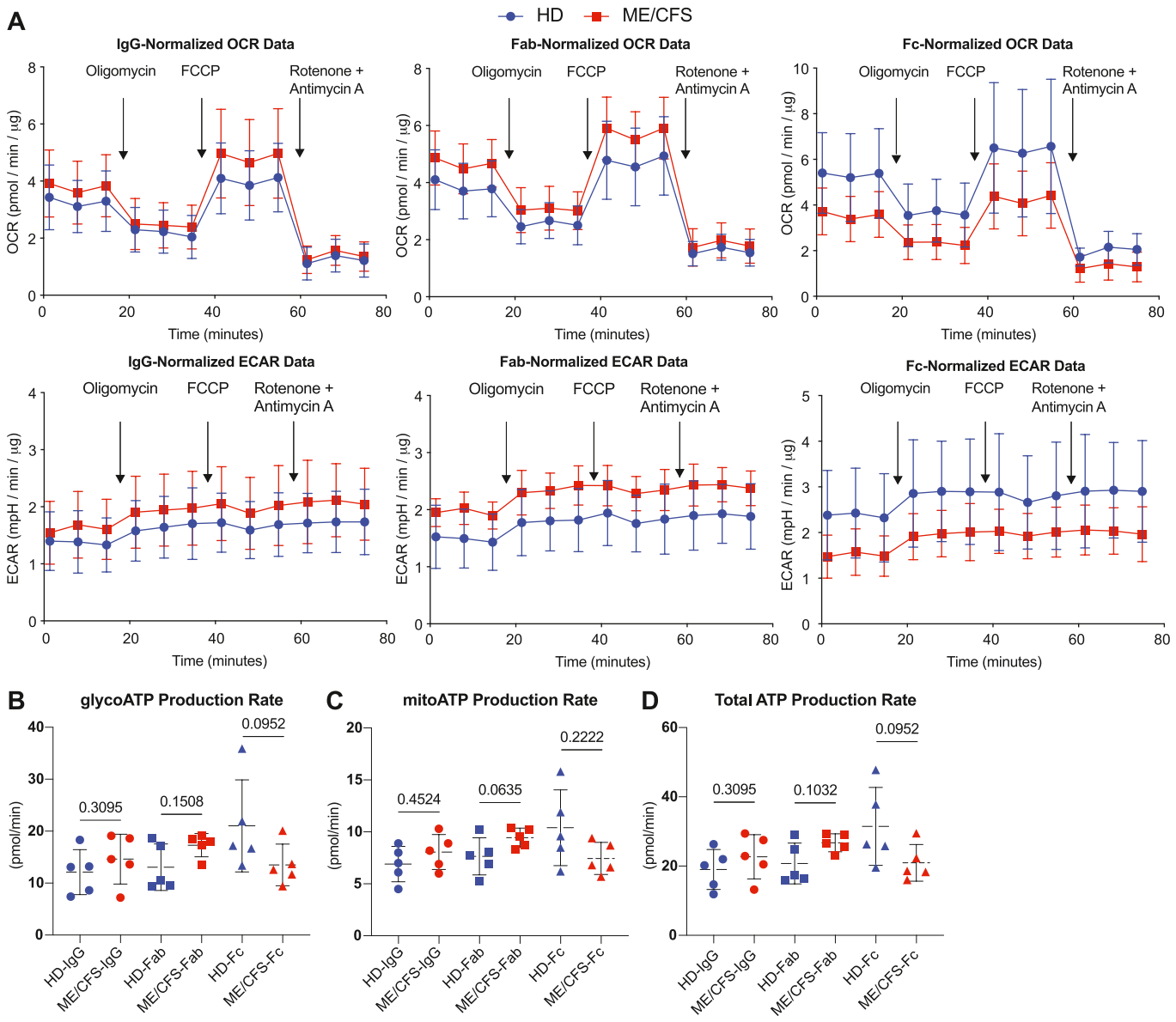


**Fig. 4. Fab and Fc fragments of IgG have variable effects on metabolic energetics in HUVECs.**

A. Normalized OCR and ECAR in HUVECs exposed to 1 µg/mL IgGs, Fab fragments, and Fc fragments from the same 5 ME/CFS and 5 healthy controls measured by Seahorse assay mito stress test.

B-D. Seahorse real-time ATP rate assay in HUVECs exposed to 1 µg/mL IgGs, Fab fragments, and Fc fragments from the same 5 ME/CFS and 5 controls.

B. Glycolytic ATP production rate. HD-IgG vs ME/CFS-IgG, ns P = 0.3095. HD-Fab vs ME/CFS-Fab, ns P = 0.1508. HD-Fc vs ME/CFS-Fc, ns P = 0.0952.

C. Mitochondrial ATP production rate. HD-IgG vs ME/CFS-IgG, ns P = 0.4524. HD-Fab vs ME/CFS-Fab, ns P = 0.0635. HD-Fc vs ME/CFS-Fc, ns P = 0.2222.

D. Total ATP production rate. HD-IgG vs ME/CFS-IgG, ns P = 0.3095. HD-Fab vs ME/CFS-Fab, ns P = 0.1032. HD-Fc vs ME/CFS-Fc, ns P = 0.0952.

identified peptide signatures, we conducted a 3D principal component analysis (PCA) that nicely separated healthy controls from all three disease groups. Although there was no clear separation among the three disease groups, ME/CFS patients clustered slightly farther from the PCS-CFS and MS groups (Fig. 6B), as indicated by specific proteins that distinguished the individual comparison groups (Fig. 6C). A fold-change analysis was conducted to identify the most significant up- and down-regulated proteins within the immune complex across different groups (Fig. 6D–G). Immune complexes from ME/CFS patients were enriched for several immunoglobulin heavy chain variable region genes (IGHVs), including IGHV1-58, IGHV4-8, IGHV3-16, IGHV3-66, and IGHV1-69-2 (Fig. 6D). Interestingly, striated muscle-enriched protein kinase (SPEG), important for muscle maintenance, a kinase involved in muscle development and calcium handling, and Carboxypeptidase N Subunit 1 (CPN1), a metalloprotease and a plasma metalloenzyme that regulates inflammatory peptides, were also increased within the immune complex of ME/CFS patients. One key protein involved in blood hemostasis, immune modulation, and vascularization, called Von Willebrand Factor (VWF) was significantly decreased within the immune complex of ME/CFS patients (Fig. 6C and D). IGHV1-58 showed increased presence within the Immune complexes of PCS-CFS patients (Fig. 6E) along with the protein kallikrein B (KLKB1). Similarly, IGHV3-16 was enriched within the immune complex of MS patients (Fig. 6F).

We hypothesized that proteins that do not typically bind to immune complexes and are elevated within immune complexes from patients with a particular disease may represent proteins targeted by disease-specific autoantibodies (Fig. 7A). Similarly, proteins that decrease within the immune complexes of a specific disease are potentially essential for the correct functioning and regulation of the immune

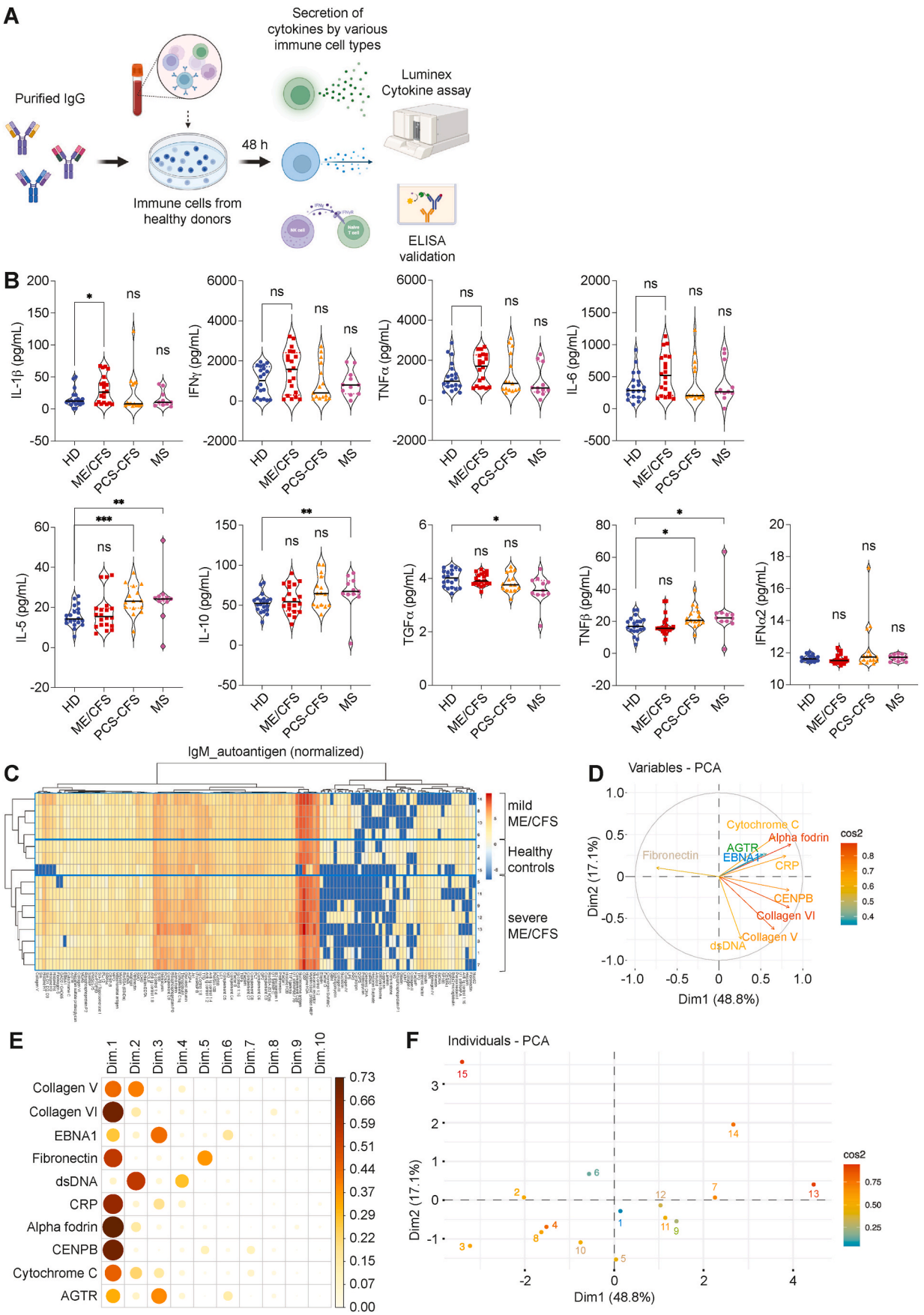


*(caption on next page)*

**Fig. 5. IgG induces inflammation and an autoantibody signature in ME/CFS.**
A. Schematics of experimental setup to measure inflammatory cytokines produced by IgG-induced inflammation.
B. Violin plots showing results of multiplex bead-based assays to measure secreted inflammatory cytokines from PBMCs of two healthy donors after 48 h of exposure of PBMCs to IgG from ME/CFS (n = 20), PCS-CFS (n = 15), MS (n = 11), and healthy donors (n = 20). Two-tailed Mann-Whitney *U* test. (IL-1β) HD vs ME/CFS, *P = 0.0460. HD vs PCS-CFS, ns P = 0.4785. HD vs MS, ns P = 0.7132. (IFNγ) HD vs ME/CFS, ns P = 0.0675; HD vs PCS-CFS, ns P = 0.9345; HD vs MS, ns P = 0.8550. (TNFα) HD vs ME/CFS, ns P = 0.1653. HD vs PCS-CFS, ns P = 0.8307. HD vs MS, ns P = 0.1566. (IL-6) HD vs ME/CFS, ns P = 0.0675; HD vs PCS-CFS, ns P = 0.9345; HD vs MS, ns P = 0.9514. (IL-5) HD vs ME/CFS, ns P = 0.8201, ***P = 0.0005; HD vs MS, **P = 0.0030. (IL-10) HD vs ME/CFS, ns P = 0.4612; HD vs PCS-CFS, ns P = 0.0545; HD vs MS, **P = 0.0016. (TGFα) HD vs ME/CFS, ns P = 0.7329. HD vs PCS-CFS, ns P = 0.2302. HD vs MS, *P = 0.0144. (TNFβ) HD vs ME/CFS, ns P = 0.6783; HD vs PCS-CFS, *P = 0.0143; HD vs MS, *P = 0.0202. (IFNα2) HD vs ME/CFS, ns P = 0.1803. HD vs PCS-CFS, ns P = 0.5366. HD vs MS, ns P = 0.7838.
C. Multivariate analysis of clusters based on distance metrics derived from IgM antibody levels for a panel of autoantigens. Log-transformed scaled data showing relative differences between different variables in both healthy controls and patients.
D. The Variables Factor map for the Principal Components (combining data from patients and healthy controls) shows the projection of the top 10 Autoantigen variables onto the plane spanned by the first two Principal Components.
E. The Contribution map shows the contributions of the top 10 Autoantigens to the top 10 dimensions.
F. Biplot of PCA analysis showing the plot of individuals for the PCA in the Fig. 5C-D.

system. These proteins may not be downregulated at the translational level. Instead, they may not be incorporated into the immune complex for some reason and, therefore, accumulate more in the serum and vice versa (Fig. 7A). To validate this, we tested serum levels of several potential proteins that were either up- or down-regulated within the immune complex. KLKB-1 protein, which showed a significantly increased presence within the immune complex of PCS-CFS patients (Fig. 6C), exhibited a trend of decreased presence in the total serum (P = 0.126) (Fig. 7B), but showed a significant decrease in the serum of ME/CFS patients (P = 0.005). AZU1, which showed reduced presence within the immune complex across all three disease groups (Fig. 6C), exhibited a trend toward increased serum levels in PCS-CSF patients (P = 0.115) (Fig. 7B). VWF levels within the immune complex showed a trend of increased presence in the total serum of PCS-CSF patients (P = 0.160) (Fig. 7B). FCN2 and serotransferrin (TF) were detected in reduced amounts within the immune complexes of all 3 disease groups and showed a significant increase in serum in these patients (Fig. 7C). The SPEG protein showed a comparative difference in its presence within the immune complex of HD and ME/CFS patients (Fig. 6C and D); however, it was barely detectable in the serum of a few patients by ELISA, making validation difficult.

We performed gene set enrichment analysis (GSEA) using the immune complex proteome data. Only one significant positive enrichment for extracellular matrix reorganization was observed in the GSEA Reactome analysis of the immune proteome in ME/CFS patients compared to healthy controls (Fig. 7D). No significant enrichment was observed in the immune proteome of PCS-CSF and MS patients. However, several significant differences were observed when the immune proteome of ME/CFS patients was compared to PCS-CSF. Gene Ontology (GO) analysis of biological processes showed a decreased response to bacterial infection in PCS-CSF patients (Fig. 7E). GSEA Reactome analysis revealed increased hemostasis (Fig. 7F), platelet activation (Fig. 7G), platelet $Ca^{2+}$ response (Fig. 7H), and fibrin clot formation (Fig. 7I) in the PCS-CSF patient immune proteome compared to ME/CFS. These results suggest specific alterations in the immune proteome of ME/CFS patients that distinguish them from healthy controls and PCS-CFS patients.

## 3. Discussions

We have recently demonstrated serum-transferrable innate immune activity in ME/CFS patients that induces a state of low mitochondrial activity, accompanied by changes in mitochondrial dynamics that may contribute to the disease's pathophysiology (Schreiner et al., 2020). Immunoglobulins are a potential candidate serum factor responsible for mitochondrial alterations. Several studies have suggested a possible role for autoantibodies in mitochondrial dysfunction (Kadaja et al., 2004; Klein and Berg, 1990). In this study, we investigated human IgG complexes as a potential serum-derived component and their roles in mitochondrial morphology, mitochondrial and cellular energetics, and inflammation. Here, we demonstrate that IgG from post-infectious ME/CFS patients induces mitochondrial fragmentation in a cell-specific manner without altering the cells' ATP-generating capacity. We showed IgG from female patients had a tendency to fragment mitochondria more effectively than IgG from male patients. This suggests that IgGs from ME/CFS and PCS-CFS patients can directly influence mitochondrial dynamics and correlate with the gender differences observed in these diseases. However, we did not observe a correlation between IgG-induced mitochondrial fragmentation and disease severity in ME/CFS and PCS-CFS (Supplementary Fig. S1). Interestingly, IgG-induced changes in mitochondrial surface area significantly predicted disease severity in patients with MS. Current results are not enough to explain these correlation results, but the physiological differences in IgG's effect on mitochondria separate MS from both ME/CFS and PCS-CFS. This also suggests that mitochondrial fragmentation is not a general feature of autoimmune conditions but may be disease-specific and involve disease-specific autoantibodies. Further analysis revealed that this mitochondrial fragmentation is not caused by excessive mitochondrial fission, which is typically mediated by Drp1. Instead, we observed a general reduction in multiple mitochondrial proteins, including Drp1, PLD6, Miga1, and mitofilin (Fig. 2D), indicating potential mitochondrial destabilization and degradation in ME/CFS, which was not observed in MS.

In our study, IgGs from ME/CFS patients induced distinct metabolic energetics, which likely connect to the mitochondrial structural changes observed earlier. IgGs from ME/CFS patients increased mitochondrial respiration and glycolytic activity (Fig. 3A), suggesting that endothelial cells were under high energy demand in the presence of IgG, a possible indication of cellular stress. To assess mitochondrial function independent of glycolysis, we replaced glucose with galactose in the assay medium, which forces cells to rely exclusively on OXPHOS. The higher spared respiration capacity induced by IgGs from ME/CFS was not displayed anymore in the presence of galactose (Fig. 3C), suggesting glycolytic compensation as a primary source of stress in ME/CFS. However, this can be cell type dependent, as HUVECs rely heavily on glycolysis. Another study has reported a significant increase in ATP production in PBMCs from ME/CFS, primarily due to non-mitochondrial respiration, such as glycolysis (Lawson et al., 2016). Here, we demonstrate that IgGs from ME/CFS exhibit greater glycolytic compensation. Elevated glycolysis could potentially lead to oxidative stress, increased ROS production (Shankar et al., 2025), and impaired energy metabolism, ultimately contributing to mitochondrial dysfunction (Hu et al., 2012; Bhatti et al., 2017). Interestingly, IgGs from PCS-CFS patients did not alter the cellular energetics to the same level as those from ME/CFS patients. Overall, ME/CFS IgGs induced mitochondrial fragmentation and metabolic stress, without necessarily impairing oxidative phosphorylation (OXPHOS) function in HUVECs. We did not observe significant alterations in IgG-induced mitochondrial ATP generation in HUVEC cells. This is expected as endothelial cells rely on glycolysis for basal energy. But they need mitochondria for other major activities,

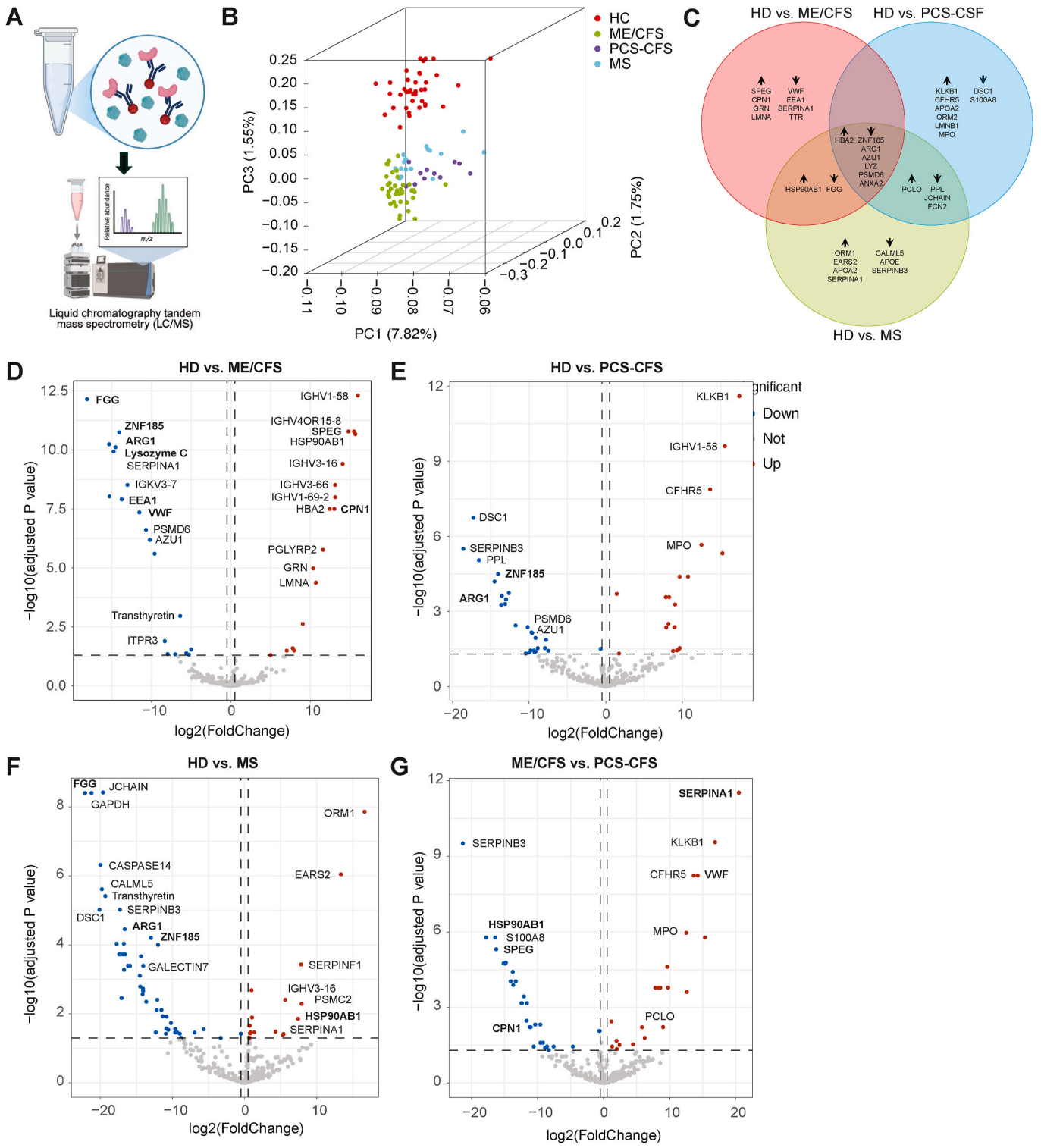


**Fig. 6. Immune proteome analysis shows distinct alterations in disease groups.**

A. Schematics of IgG-bound immune complex mass spectrometry-based proteomics.

B. 3-Dimensional Principal Component Analysis (PCA) showing distribution of various disease groups and healthy controls on 3 different axis (PC1, PC2, and PC3). ME/CFS (n = 39), PCS-CFS (n = 15), MS (n = 11) patients, and healthy controls (n = 41).

C. Venn diagram showing differentially detected proteins and commonly detected proteins within individual comparison groups as detected from mass spectrometry analysis of the immune proteome.

D-G. Volcano plots of log2 fold changes and log10 adjusted P values for individual proteins detected by mass spectrometry. Top candidate genes upregulated (red) or downregulated (blue) with logFC >1 and adjusted P value < 0.05 are indicated.

Differentially detected proteins between healthy controls (HD) and ME/CFS (D), HD vs PCS-CFS (E), HD vs MS (F), and ME/CFS vs PCS-CFS (G). (For interpretation of the references to colour in this figure legend, the reader is referred to the Web version of this article.)

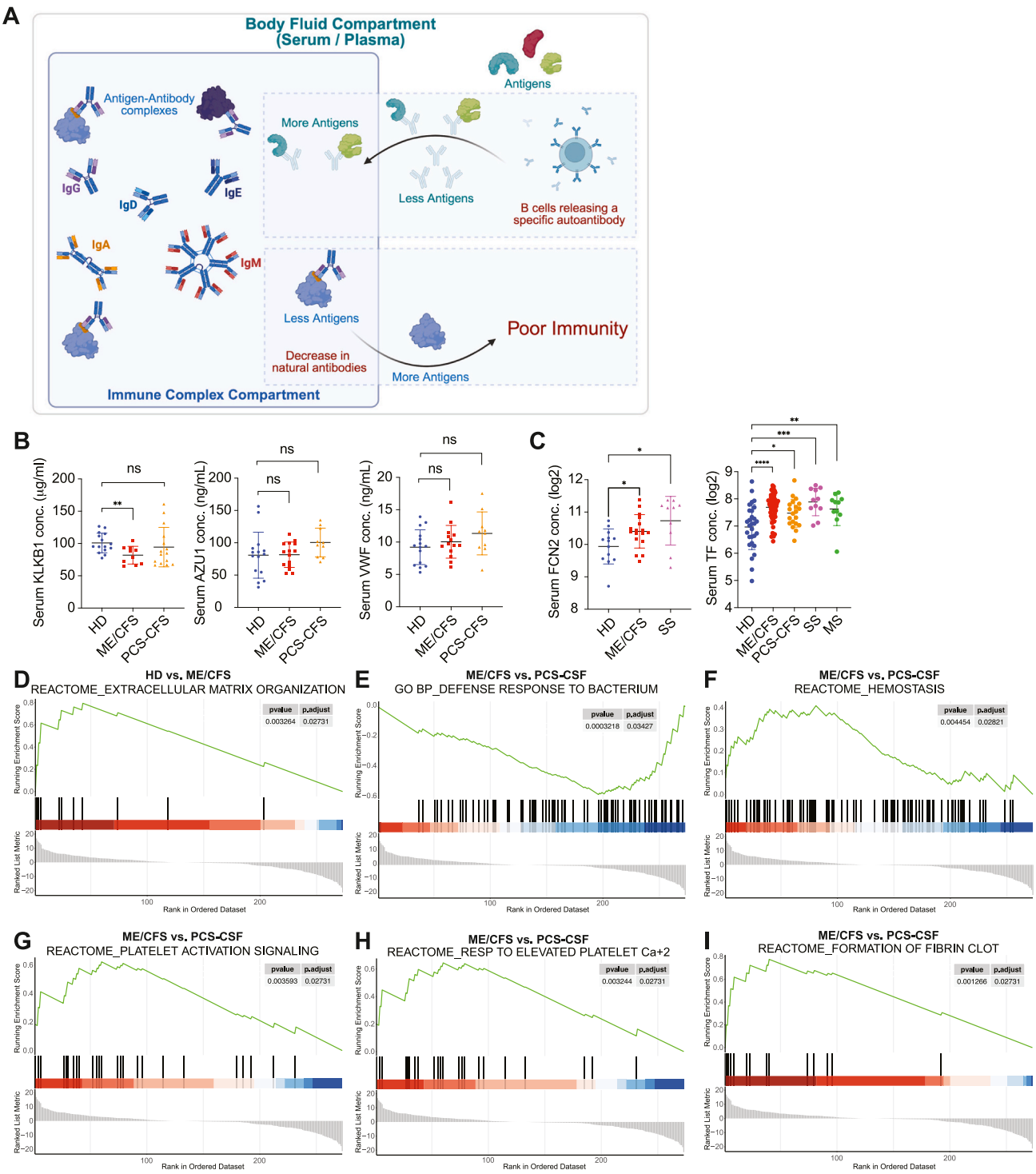


**Fig. 7. Gene Set Enrichment Analysis (GSEA) identified key altered pathways in patients with ME/CFS.**

A. Schematics showing potential alterations within antigen-antibody complexes and their effect on immunity.

B. Serum KLKB1, AZU1, and VWF levels in healthy controls, ME/CFS, and PCS-CFS patients. Two-tailed Mann-Whitney *U* test. (KLKB1) HD vs ME/CFS, **P = 0.0046. HD vs PCS-CFS, ns P = 0.1286. (AZU1) HD vs ME/CFS, ns P = 0.5123. HD vs PCS-CFS, ns P = 0.1054. (VWF) HD vs ME/CFS, ns P = 0.3705. HD vs PCS-CFS, ns P = 0.1642.

C. Serum FCN2 and TF levels in healthy controls, ME/CFS, PCS-CFS, Systemic Sclerosis (SS) and Multiple Sclerosis (MS) patients. Two-tailed Mann-Whitney *U* test. (FCN2) HD vs ME/CFS, *P = 0.0287. HD vs SS, *P = 0.0104. (TF) HD vs ME/CFS, ****P < 0.0001. HD vs PCS-CFS, *P = 0.0191. HD vs SS, ***P = 0.0008. HD vs MS, **P = 0.0087. D. GSEA Reactome analysis of the immune proteome identified enhanced extracellular matrix organization in ME/CFS patients compared to healthy controls.

E. Gene Ontology (GO) analysis of biological processes in the immune proteome identified a reduced defense response to bacterial pathogens in PCS-CFS patients compared with ME/CFS patients.

F-I. GSEA Reactome analysis of the immune proteome identified increased hemostasis (F), platelet activation and signalling (G), response to elevated platelet-derived cytosolic Ca+2 (H), formation of fibrin clot (I) in PCS-CFS patients compared to ME/CFS patients.

including redox regulation, stress adaptation, angiogenesis, and responses to shear stress. Mitochondrial alterations could block these adaptive mechanisms, making endothelial cells unable to respond to increased metabolic demand (e.g., during exertion) and, in turn, driving PEM-like physiology.

Immune complex proteomics specifically isolates antibody-bound proteins, enriching for antigens, autoantigens, and immune mediators. While plasma proteomics provides a broader overview of circulating proteins, immune complex proteomics offers a more targeted and enriched assay for studying autoimmune diseases, where immune activity plays a dominant role in disease progression and treatment outcomes (Ohyama et al., 2015). Our immune proteome analysis revealed specific changes in the immune complex of ME/CFS patients compared to healthy controls and other disease controls, which may be relevant to many of ME/CFS's clinical features. We observed increased SPEG protein amounts within the immune complex of ME/CFS patients (Fig. 6C and D), suggesting the presence of autoantibodies against SPEG in ME/CFS. SPEG are muscle-expressed protein kinases. They play an essential role in muscle differentiation and maintenance (Hsieh et al., 2000). Loss of SPEG results in structural muscle defects, including mislocalization of focal adhesion proteins and abnormal calcium handling, which could potentially contribute to the pathophysiology in ME/CFS (Luo et al., 2021). SPEG is mostly intracellular, found in cardiac and skeletal muscle cells (Hsieh et al., 2000). It is unlikely to be found in significant amounts in serum samples. However, in the event of muscle or cardiac injury, SPEG may be released into the serum (Martinez-Amat et al., 2005). We demonstrated a decreased presence of VWF proteins within the immune complexes of ME/CFS and concurrently validated their concurrent increase in serum. VWF is primarily involved in hemostasis by mediating platelet adhesion and stabilizing coagulation Factor VIII, thereby initiating clot formation (Federici, 2011). Additionally, VWF binds to C1q, reducing phagocytosis and pro-inflammatory cytokine secretion by macrophages (Donat et al., 2019). Studies have shown that VWF plays a role in regulating blood vessel formation and in vascular dysregulation (Randi and Laffan, 2017). In ME/CFS, dysfunction in these processes has been reported (van Campen et al., 2023). We detected reduced levels of several key proteins, including AZU1, ARG1, ZNF185, and LYZ, within the immune complexes of all three disease groups (Fig. 6C), suggesting a potential common role of IgGs in immune dysfunction and autoimmunity.

Our immune proteome analysis revealed several significant alterations in pathways and biological processes. Only one significant alteration (extracellular matrix (ECM) organization) was predicted in ME/CFS patients through GSEA Reactome analysis (Fig. 7A). In a previous study, we demonstrated a significantly elevated serum fibronectin (FN1) level in both ME/CFS and post-COVID patients, but not in MS patients (Liu et al., 2023). In this study, FN1 was detected at lower levels in the immune complexes of a subset of patients. Alterations in ECM can lead to neuroinflammation (Sorokin, 2010), vascular dysfunction (Zhang et al., 2025), mitochondrial dysfunction (Zhang et al., 2024), fibrosis, and tissue stiffness (Herrera et al., 2018; He et al., 2024). The ECM is essential in maintaining vascular integrity and permeability. Dysregulation of the ECM could lead to capillary leakage, inadequate tissue perfusion, and altered mechanotransduction signaling in endothelial cells, resulting in orthostatic intolerance, postural orthostatic tachycardia syndrome (POTS), and other signs of microvascular dysregulation commonly observed in ME/CFS patients. The ECM may act as a regulatory interface among the immune, nervous, and vascular systems in ME/CFS. Aberrant ECM remodeling could be a downstream effect of chronic inflammation, infection, or autoimmunity, and in turn, perpetuates the disease cycle. We did not observe similar pathway enrichments for PCS-CFS patients. However, several key differences were predicted between ME/CFS and PCS-CFS groups, including lower antibacterial defense, increased hemostasis, platelet activation and signaling, and fibrin clot formation (Fig. 7B–F). These pathways were enriched in the PCS-CFS groups compared to the ME/CFS group. All these processes are altered in post-COVID patients and have been an intense topic of study recently (Davis et al., 2023). Our results demonstrate the potential for developing disease markers based on the proteome of immune complexes. However, more data and in-depth studies are required to validate some of these markers.

SARS-CoV-2 infection-induced ME/CFS (PCS-CFS) patients share clinical features with ME/CFS patients with unknown etiology. Our study offers a biological perspective for comparing various molecular aspects of these two conditions. While IgG-induced mitochondrial fragmentation and alteration in energetics were more prominent in post-infectious ME/CFS patients, IgG-induced alterations in inflammation-associated cytokines were prominent in PCS-CFS patients. IgG proteomics also showed distinct signatures within the immune complex of these two groups. We hypothesize that PCS-CFS patients represent an early stage of ME/CFS, where inflammation dominates clinical outcomes, whereas ME/CFS patients represent the chronic nature of the disease, characterized by hypometabolism and consequent metabolic alterations that influence clinical presentation. In summary, our data provide a mechanistic basis for considering therapeutic strategies targeting autoantibody-mediated pathology.

## 4. Methods

### 4.1. Experimental methods

Details of key resources are provided in the form of a table within Supplementary methods.

#### 4.1.1. Patient recruitment and serum collection

Postinfectious ME/CFS, including post-COVID ME/CFS (PCS-CFS) patients, relapsing-remitting multiple sclerosis (MS) patients, and gender- and age-matched healthy controls, were recruited at the outpatient clinic of the Charité Universitätsmedizin, Berlin, between 2020 and 2023. The diagnosis of ME/CFS was based on the 2003 Canadian Consensus Criteria and on the exclusion of other medical or neurological diseases that may cause fatigue through a comprehensive clinical and laboratory evaluation. MS patients have been suffering from fatigue relevant to everyday life and have to be free from relapses as well as from steroid treatment for at least 6 months. Biosamples of ME/CFS patients and healthy controls were collected by the group of Prof. Scheibenbogen, and biosamples of MS patients were collected by the group of Prof. Paul. The study was approved by the Ethics Committee of Charité Universitätsmedizin Berlin (EA2/067/20; EA2_066_22; EA4_174_22) in accordance with the 1964 Declaration of Helsinki and its subsequent amendments, as well as by the Medizinische Ethikkommission of JMU, Würzburg (83/23). A total of 21 serum samples from patients diagnosed with systemic sclerosis were collected by the group of Prof. Riemekasten at the Clinic for Rheumatology and Clinical Immunology, University Hospital Schleswig-Holstein, Lübeck, Germany, as part of the same approved study. These samples were only used for potential biomarker validation. All donors gave informed consent. Whole blood samples from each subject were allowed to clot at room temperature, then centrifuged at 2000×*g* for 10 min. The serum was stored in aliquots at −80 °C. Patient demographic is presented in Supplementary Table 1.

#### 4.1.2. Cell culture

U2-OS (HTB-96) cells were purchased from ATCC, and HUVEC-TERT2 cells (CHT-006-0008) were purchased from Evercyte, Austria. Human foreskin fibroblast cells (HFF-TERT) were kindly provided by Prof. Michael Weekes (Cambridge Institute for Medical Research, University of Cambridge, UK). U2-OS and HFF-TERT cells were grown in McCoy's 5A (Gibco, 16600082) and DMEM media (Gibco, 11965092), respectively, supplemented with heat-inactivated 10% fetal bovine serum (FBS) (Sigma-Aldrich, S0615) and 1% penicillin-streptomycin (Gibco, 15140122). HUVEC-TERT2 cells were grown in EBM basal

medium (Lonza, Cat#CC-3121) supplemented with Components of EGM SingleQuot Kit (Lonza, Cat# CC-4133: BBE, hEGF, hydrocortisone, ascorbic acid), 10% FBS, and 20 μg/ml G418. All cell lines were cultured at 37 °C with 5% CO2. Cells carrying stable GFP expression in mitochondria were developed as described previously (Hennig et al., 2022). Cells stably expressing GFP were created by cloning the mitochondrial-targeted GFP into pLVTHM vector backbone and transducing target cells with the lentivirus as mentioned before (*50*). All cell lines were frequently tested for Mycoplasma contamination and, where necessary, authenticated by sequencing.

#### 4.1.3. Immunoglobulin purification

150 μl Protein G Sepharose 4 Fast Flow (#17061801, Cytiva) was loaded onto Poly-Prep Chromatography Columns (#731-1550, BIO-RAD). After washing the beads with PBS, 500 μL of serum sample was loaded and passed through the column three times, which was followed by three washes with PBS. Protein G-bound serum IgG was eluted by Glycine pH 2.7 and then neutralised with 1M Tris-HCl pH 8.0. IgG elute was dialyzed against PBS in Slide-A-Lyzer MINI Dialysis Devices (#88404, Thermo Fisher Scientific). IgG concentration was measured by Easy-Titer Human IgG (H + L) Assay Kit (#23310, Thermo Fisher Scientific).

#### 4.1.4. Fab fragments purification

Fab fragments of immunoglobulin G were purified using the Pierce Fab Micro Preparation Kit (#44685, Thermo Fisher Scientific), according to the manufacturer's protocol. Fab fragments and flow-through containing digested Fc fragments were dialyzed against PBS in Slide-A-Lyzer MINI Dialysis Devices (#88401, Thermo Fisher Scientific). The concentrations of these fragments were quantified using a NanoDrop™ 2000 Spectrophotometer (Thermo Fisher Scientific).

#### 4.1.5. IgG exposure in cell culture

U2-OS or HUVEC-TERT2 cells carrying soluble mitoGFP were seeded on 6-well plates and cultured overnight. Cell culture medium was replaced by fresh medium containing 1 μg/ml serum IgG or 0.5 μg/ml Fab fragments or flow-through, allowing cells to be exposed to serum-derived IgG, Fab fragments, or flow-through containing Fc fragments. Cells were collected after 16 h and 36 h for Western blot or immunofluorescence experiments.

#### 4.1.6. Fc receptor blocking assay

One hour prior to IgG exposure, the cell culture medium was replaced with fresh medium containing (20 μL) Azide Free Fc Receptor Blocker (#NB335, Innovex Biosciences). Following incubation, an equal volume of culture medium containing 2 μg/mL serum IgG was added to each well.

#### 4.1.7. Immunofluorescence microscopy

Cells were seeded in 12-well plates on glass coverslips overnight and exposed to IgG. Cells were washed in PBS and fixed with 4% paraformaldehyde for 30 min. After washing, the cells were permeabilized with 0.2% Triton X-100 in PBS for 10 min and blocked with 10% FCS in PBS for 1 h. Cells were then incubated for 1 h with Anti-Human IgG (H + L) CF594 (#SAB4600097, Sigma-Aldrich) in 2% FCS-PBS and washed 3 times in PBS. DAPI was used for staining cell nuclei. When GFP mitochondria and DAPI are the only channels required, the DAPI staining was followed directly after fixation. Samples were mounted onto slides using ProLong Glass Antifade Mountant with NucBlue Stain (#P36981, Invitrogen). Samples were analyzed on a confocal microscope (LSM 510 Meta, Carl Zeiss AG).

#### 4.1.8. Average mitochondrial surface area and mitochondrial number analysis

Software and a modified algorithm for mitochondrial size and number measurement were previously described by us in detail (Hennig et al., 2022; Chowdhury et al., 2017). All image-processing and analysis steps were performed using Fiji (Schindelin et al., 2012).

#### 4.1.9. Immunoblotting

Immunoblotting was carried out as described before (Gulve et al., 2016; Prusty et al., 2018) using antibodies: Drp1 antibody (#sc-101270, Santa Cruz Biotechnology), Mfn1 antibody (#sc-166644, Santa Cruz Biotechnology), Mfn2 antibody (#sc-515647, Santa Cruz Biotechnology), PLD6 antibody (#ab237612, Abcam), FAM73A Antibody (#PA553611, Invitrogen), p53 antibody (#sc-126, Santa Cruz Biotechnology), TOMM20 antibody (#sc-17764, Santa Cruz Biotechnology), TIMM23 antibody (#sc-514463, Santa Cruz Biotechnology), LC3β antibody (#sc-376404, Santa Cruz Biotechnology). Equal protein loading was confirmed by the following antibodies: Actin antibody (#sc-8432, Santa Cruz Biotechnology) and Vinculin antibody (#sc-73614, Santa Cruz Biotechnology). All primary antibodies were used at a dilution of 1:1000 to 1:3000. HRP-conjugated secondary antibodies, which are HRP Rabbit Anti-Human IgG (whole molecule) (#A8792, Sigma-Aldrich), Goat Anti-Human IgG (Fc specific) HRP (#A0170, Sigma-Aldrich), Goat Anti-Mouse IgG Antibody, HRP-conjugate (#12-348, Sigma-Aldrich), and Goat Anti-Rabbit IgG Antibody, HRP-conjugate (#12-349, Sigma-Aldrich), were used at a dilution of 1:2000 to 1:10,000.

1 μL of HUVEC protein lysates after IgG exposure were run in parallel on an automated capillary Simple Western (JESS from Bio-Techne) for proper quantification. Simple Western was performed according to the manufacturer's protocol using 12-230 kDa (#SM-W004, Bio-Techne) or 2-40 kDa (#SM-W004, Bio-Techne) separation modules with chemiluminescent Anti-Mouse (#DM-002, Bio-Techne), Anti-Rabbit (#DM-001, Bio-Techne) or fluorescent Anti-Mouse (#DM-009, Bio-Techne), Anti-Rabbit (#DM-007, Bio-Techne) detection modules, and results were analyzed using Compass software (version 6.3.0). Assays were performed using antibodies: Mitofilin antibody (#ab245764, Abcam), Drp1 antibody (#sc-101270, Santa Cruz Biotechnology), TIMM23 (#sc-514463, Santa Cruz Biotechnology), PLD6 antibody (#ab237612, Abcam), FAM73A (Miga1) Antibody (#PA553611, Invitrogen), LC3β antibody (#18725-1-AP, Proteintech), PINK1 antibody (#NB100-644, Novus Biologicals). Equal protein loading was confirmed by Vinculin antibody (#sc-73614, Santa Cruz Biotechnology). All primary antibodies were used at a dilution of 1:50 to 1:500.

#### 4.1.10. Seahorse assay extracellular flux analysis

Mitochondrial function was assessed using the Seahorse XF Cell Mito Stress Test on the XFe96 Extracellular Flux Analyzer (Seahorse Bioscience). XFe96/XF pro cell culture microplates (#103793-100, Agilent) were pre-coated with 0.1% gelatin (#0646.1, Carl Roth) and seeded with 4000 HUVECs per well. After overnight incubation, cells were exposed to purified serum IgG for 16 h. All experimental conditions were performed in triplicate. On the day of the assay, the culture medium was replaced with Seahorse XF RPMI medium (#103576-100, Agilent), supplemented with 10 mM D-glucose (#G8769, Sigma Aldrich), 2 mM L-glutamine (#A2916801, Gibco), and 1 mM sodium pyruvate (#11360070, Gibco), and adjusted to pH 7.4. When required, 10 mM D-glucose was replaced to 10 mL D-Galactose (#G5388, Sigma Aldrich). Plates were incubated for 1 h at 37 °C in a non-$CO_2$ incubator prior to measurement. The Mito Stress Test was conducted according to the manufacturer's instructions. Briefly, baseline oxygen consumption rate (OCR) and extracellular acidification rate (ECAR) were measured, followed by sequential injections of 1.5 μM oligomycin (ATP synthase inhibitor), 1.0 μM FCCP (mitochondrial uncoupler), and 0.5 μM rotenone combined with 0.5 μM antimycin A (Complex I and III inhibitors, respectively). Each injection step included three measurement cycles, each comprising a mixing and a measuring phase. Following the Seahorse assay, cells were lysed in 0.1 M NaOH containing protease inhibitors and incubated at room temperature for 10 min. Protein concentration was quantified using Pierce BCA Protein Assay Kit

(#23225, Thermo Fisher Scientific) according to the manufacturer's protocol, for normalization of Seahorse assay data. Seahorse assay data were recorded, processed, and analyzed using software Wave (Agilent). Mito Stress Test reports were generated according to the Seahorse XF Cell Mito Stress Test Report Generator template. OCR and ECAR values were analyzed to calculate key mitochondrial parameters, including basal respiration, ATP-linked respiration, proton leak, maximal respiration, spare respiratory capacity, and non-mitochondrial respiration. To quantify ATP production rates, the same Seahorse data set from the Mito Stress Test was reanalyzed using Seahorse XF Real-Time ATP Rate Assay Report Generator. OCR and ECAR values obtained before and after injection of oligomycin and rotenone/antimycin A were used to calculate mitochondrial ATP production, glycolytic ATP production, and total ATP production rates.

For experiments related to Fig. 3 and Supplementary Fig. S2A–S2B, we have separated ME/CFS patients into two arbitrary subgroups. This separation is based on the mitochondrial surface area quantification data shown in Fig. 2B. IgGs that induce strong mitochondrial fragmentation show reduced average mitochondrial surface area. For the experimental results shown in Fig. 3A–B, we randomly selected 10 ME/CFS patients from the group that exhibited a reduction in average mitochondrial surface area relative to the mean surface area of healthy controls. For the experimental results shown in Fig. S2A–S2B, we randomly selected 10 ME/CFS patients from the group that did not alter or increase mitochondrial surface area compared to healthy controls.

#### *4.1.11. IgG-induced inflammation assay using human PBMCs*

a. Experimental setup

Peripheral blood was obtained from an apparently healthy adult donor under the ethical approval of Riga Stradiņš University (RSU) Research Ethics Committee (2-PĒK-4/784/2025). PBMCs were isolated by density gradient centrifugation using Histopaque-1077 (Sigma-Aldrich, Cat# 10771) according to the manufacturer's instructions. After centrifugation, the PBMC layer was collected, washed twice with sterile phosphate-buffered saline (Sigma-Aldrich, Cat# D8537), and resuspended in complete RPMI 1640 medium (ThermoFisher Scientific, Cat# 22400-089) supplemented with 10% heat-inactivated, filtered fetal bovine serum (FBS) and 1% Penicillin-Streptomycin.

Cells were seeded in flat-bottom 96-well plates (Sarstedt, Cat# 83.1835.300) at a density of $2 \times 10^5$ cells per well in 200 µL of culture medium. Dialyzed IgG (final concentration: 50 µg/mL) from serum samples of healthy controls, patients with ME/CFS, PCS-CFS, or MS was added to the freshly isolated PBMCs immediately upon plating. Cells were incubated at 37 °C in a humidified atmosphere containing 5% $CO_2$ for 48 h. Following incubation, culture supernatants were collected and centrifuged at 400×*g* for 5 min to remove cell debris. Concentrations of interleukin-6 (IL-6), interleukin-1β (IL-1β), and tumor necrosis factor alpha (TNF-α) were measured using commercially available enzyme-linked immunosorbent assay (ELISA) kits (ThermoFisher Scientific: IL-6, Cat# 88-7066-88; IL-1β, Cat# 88-7346-88; TNF-α, Cat# 88-7261-88) following the manufacturer's protocols. Absorbance was measured at 450 nm using a microplate reader (ThermoFisher, Varioskan LUX), and cytokine concentrations were calculated from standard curves generated with recombinant standards provided in each kit.

b. Multiplex bead-based assay for inflammatory marker measurements

The cell culture supernatant from PBMCs was centrifuged at 5000 g for 5 min to obtain a cell- and debris-free supernatant. TNF-α, IFNγ, IL-5, IL-10, IL-6, IL-1β, IFNα2, sCD40L, TGFα, and TNF-α levels in cell culture supernatants were quantified using the Milliplex MAP Human Cytokine, Chemokine, and Growth Factor Panel A Magnetic Bead Panel kit (HCYTA-60K, Millipore) according to the manufacturer's protocol. Briefly, the samples were combined with marker-specific antibody-coupled magnetic beads in a 96-well plate and incubated overnight at 4 °C. Following incubation, the plate was washed on a magnet, followed by incubations with biotinylated detection antibodies and streptavidin-phycoerythrin. Finally, the plate was washed on a magnet, and beads were resuspended in xMAP Sheath Fluid Plus (40-50021, Luminex). The plate was read using the Luminex 200 instrument and xPONENT software, and the results were analyzed using GraphPad Prism to construct a 7-point standard curve using a 5-parameter logistic curve-fitting method. Each plate included a background and two quality controls. Before reading the plate, the Luminex 200 instrument was calibrated and verified using the Luminex 100/200 Calibration and Performance Verifications kits (LX2R-CAL-K25 and LX2R-PVER-K25, Luminex). Each IgG was tested in two separate biological replicates per PBMC sample. Two such independent experiments were carried out using separate donor-derived PBMCs. The obtained results were combined, and the average values for each cytokine were used.

#### *4.1.12. Mass spectrometry*

a. Mass spectrometry sample preparation

A fraction of serum IgG-bound protein G beads from IgG purification was eluted by NuPAGE LDS Sample Buffer (4X) (#NP0007, Thermo Fisher Scientific). The eluates were sent for mass spectrometry.

b. Single-pot, solid-phase-enhanced sample preparation (SP3)

Samples were processed using an adapted SP3 protocol (Hughes et al., 2019). Briefly, 200 µl reconstitution solution was added to each sample prepared in 50 µl NuPAGE LDS sample buffer (Life Technologies). Reduction was performed using 5 mM DTT, followed by alkylation with 20 mM iodoacetamide. 10 mM additional DTT was used for quenching. Equal volumes of two types of Sera-Mag Speed Beads (Cytiva, #45152101010250 and #65152105050250) were combined, washed with water, and 10 µL of the bead mix was added to each sample. 260 µl 100% ethanol was added, and samples were incubated for 5 min at 24 °C, 1000 rpm. Beads were captured on a magnetic rack for 2 min, and the supernatant was removed. Beads were washed twice with 200 µl of 80% ethanol (Chromasolv, Sigma) and once with 1000 µl of 80% ethanol. Digestion was performed on beads with 0.25 µg Trypsin (Gold, Mass Spectrometry Grade, Promega) and 0.25 µg Lys-C (Wako) in 100 µl 100 mM ammonium bicarbonate at 37 °C overnight. Peptides were desalted using C-18 Stage Tips (Rappsilber et al., 2003). Each Stage Tip was prepared using three C-18 Empore SPE Discs (3 M) in a 200 µl pipette tip. Peptides were eluted with 60 % acetonitrile in 0.1 % formic acid, dried in a vacuum concentrator (Eppendorf), and stored at −20 °C. Peptides were dissolved in 2 % acetonitrile/0.1 % formic acid prior to nanoLC-MS/MS analysis.

c. NanoLC-MS/MS analysis

NanoLC-MS/MS analyses were performed on an Orbitrap Fusion (Thermo Scientific) equipped with a PicoView Ion Source (New Objective) and coupled to an EASY-nLC 1000 (Thermo Scientific). Peptides were loaded on a trapping column (2 cm × 150 µm ID, PepSep) and separated on a capillary column (30 cm × 150 µm ID, PepSep) both packed with 1.9 µm C18 ReproSil and separated with a 120-min linear gradient from 3% to 30% acetonitrile and 0.1 % formic acid and a flow rate of 500 nl/min. Both MS and MS/MS scans were acquired in the Orbitrap analyzer with a resolution of 60,000 for MS scans and 30,000 for MS/MS scans. HCD fragmentation with 35 % normalized collision energy was applied. A Top Speed data-dependent MS/MS method with a fixed cycle time of 3 s was used. Dynamic exclusion was applied with a repeat count of 1 and an exclusion duration of 90 s; singly charged precursors were excluded from selection. The minimum signal threshold

for precursor selection was set to 50,000. Predictive AGC was used with AGC a target value of $4 \times 10^5$ for MS scans and $5 \times 10^4$ for MS/MS scans. EASY-IC was used for internal calibration.

d. Mass spectrometry data analysis

Raw mass spectrometry data files were analyzed with MaxQuant version 1.6.2.2 (Cox and Mann, 2008). A database search was performed using Andromeda, integrated into the version of MaxQuant used. The search was performed against the UniProt Human Reference Proteome database (Release, 2024_3, UP000005640, 82518 entries), the UniProt EBV database (Release, 2024_3, UP000272970, 55 entries), and the UniProt HHV-6A database (Release, 2024_3, UP000009295, 99 entries). Additionally, a database containing common contaminants was used. The search was performed with trypsin cleavage specificity, allowing up to 3 miscleavages. Protein identification was controlled by the false-discovery rate (FDR; <1% FDR at the protein and peptide spectrum match (PSM) levels). In addition to the MaxQuant default settings, the search was performed against the following variable modifications: Protein N-terminal acetylation, Gln-to-pyro-Glu formation (N-terminal Gln), and oxidation (Met). Carbamidomethyl (Cys) was set as a fixed modification. LFQ intensities were used for protein quantitation (Cox et al., 2014).

The raw MaxQuant output files revealed expression data for 783 proteins. We focused on raw intensity values and label-free quantification (LFQ) intensity values for further analysis. The data processing and analysis work consisted of 4 components: Data processing, Clustering and PCA, Differential expression analysis, and pathway enrichment analysis. The first step of data processing involved contaminant filtering, removing proteins with excessive missing values, imputing missing values, and applying a log transformation. We removed contaminants and low-quality proteins from the MaxQuant output data. Proteins filtered out included those with Potential contaminant value +, Reverse value +, and site value +. Locally developed Python code was used for this purpose. To remove proteins with excessive missing values, we removed proteins with raw intensity values equaling 0 for at least 70% of the samples within the group. Missing values were evaluated using plots generated with the Amelia (v1.8.1) R package's missmap (.) function, with default parameters. Imputation was performed on LFQ intensity data, although proteins with missing values were identified based on raw intensity. Specifically, when the raw intensity value for a protein was 0, it was considered a missing value; subsequently, the LFQ intensity was imputed. If samples with missing values exceeded 70% of all samples within a group, the LFQ intensity values were imputed to be 0. If samples with missing values did not exceed 70% of all samples within a group, KNN imputation was performed. The scikit-learn (v0.23.2) Python package was invoked, using the KNNImputer function, which was applied with the neighbor number (k) set to the sample size for the group. Locally developed Python code was used to summarize the results.

Log transformation (base 2) was performed for imputed LFQ intensity values using locally developed Python code. Data were visualized using density distributions and box plots, generated with the Matplotlib Python package (version 3.7.5). Hierarchical clustering analysis was performed for all proteins using the pheatmap (version 1.0.12) R package. ggplot2 (v3.5.1) R package was used to generate clustering plots. PCA was performed using the gmodels R package (version 2.19.1). ggplot2 (v3.5.1) and scatterplot3d (v0.3.44) R packages were used to generate 2D and 3D PCA plots, respectively.

Differential expression analysis was performed using the limma (version 3.62.1) R package. The volcano plot was generated using ggplot2 (v3.5.1) R packages. Heatmaps of differentially expressed proteins were generated using the pheatmap (version 1.0.12) R package. GSEA was performed using the fgsea (version 1.32.2) and clusterProfiler (version 4.14.4) packages. An adjusted P-value <0.05 was used to select significant enrichment pathways. Pathway enrichment analysis was carried out to identify enriched GO terms among up- and down-regulated proteins using the DAVID (v2023q4) web tools (https://davidbioinformatics.nih.gov/). A FDR cut-off of 0.05 was adopted to select significant pathways. ggplot2 (v3.5.1) R package was used to generate bubble plots. Gene set enrichment analysis (GSEA) using Gene Ontology (GO) terms, including Biological Process (BP), Cellular Component (CC), and Molecular Function (MF), as well as using the Reactome dataset, for the six pair-wise comparisons between the four groups of samples. Four GSEA sets were conducted for each of the 6 pairwise comparisons, for a total of 24 sets of analysis attempted.

e. Enzyme-Linked Immunosorbent Assay (ELISA)

ELISA was performed using the following kits according to the manufacturers' protocols: Human Ficolin-2 ELISA Kit (#EH192RB, Invitrogen), Transferrin ELISA Kit (#EHTF, Invitrogen), Human Prekallikrein 1B ELISA Kit (#ab202405, Abcam), Human Azurocidin/CAP37 ELISA Kit (#EH39RB, Invitrogen) and Human von Willebrand Factor (VWF) ELISA Kit (#EHVWF, Invitrogen).

#### *4.1.13. Antigen microarray pilot study*

a. Antigen Microarray experimental setup

Microarray studies for IgG and IgM against autoantigens were carried out in collaboration with Creative Biolabs, USA. Frozen serum samples without a prior freeze-thaw cycle were used for the assay. Each serum was digested with DNase I for 30 min at room temperature on a shaker. For the control, no serum sample was added. Slides carrying antigens against 120 autoantigens (for details of the antigens, please see Supplementary Table 2) were blocked in 100 μL blocking buffer at room temperature for 30 min on a shaker. Afterwards, the slides were washed twice with PBST, each for 5 min. 90 μl PBST was added to each serum sample or control mix. Diluted samples were added to each well of the slide (100 μl each) and incubated at room temperature for 1 h on a shaker. Slides were washed with 100 μl PBST/well for 5 min on the shaker. Subsequently, slides were washed with blocking buffer 100 μl/each well for 5 min on a shaker and then with PBST 100 μl/each well) for 5 min on a shaker. Anti-human IgM secondary antibody was diluted to 1:1000 in PBST, and 100 μl of secondary antibody was added to each well. Slides were incubated at room temperature for 1 h on the shaker, then washed 3 times with 100 μL PBST per well, 5 min on the shaker. Slides were then washed twice each: first with 45 ml PBS in a 50 ml tube for 5 min on the shaker, then with 45 ml nuclease-free water in a 50 ml tube for 5 min on the shaker. GenePix 4000B microarray systems were used to scan the slide. The 532 nm channel was used to scan Cy3 fluorescence, and the 635 nm channel was used to scan Alexa Fluor-647 fluorescence.

b. Microarray data analysis

Each chip had serially diluted anti-IgM and IgM as positive controls to monitor the experimental process, and PBS was used as a negative control. The obtained chip image was read using the LuxScan 3.0 software to extract the original data. Statistical tests were then carried out on the chip background and on the signal intensities of the positive and negative control sites. The results showed that the Ig control signal value was higher and uniform across different samples. In addition, the PBS anti-Ig control and background signal values were both low, meeting the quality control requirements. The chip of the test sample was scanned with the LuxScan 10K-B scanner. The autoantigen microarray chip/Pathogen-associated antigen microarray chip had 256 points in total. After removing the 8 anti-IgM and 8 Ig control points, 240 data points were obtained. Each protein on the chip was present as two technical repetitions, representing 120 autoantigens. The chip is read by LuxScan 3.0 software to obtain the original data, including foreground signal (F

Median), background signal (B Median), and so on. Foreground Median, Background Median columns were extracted from the.LSR file. The fluorescence intensity value of each site was calculated by the formula: Net Fluorescence Intensity (NFI) Value = (Foreground Median - Background Median); SNR = (Foreground Median - Background Median)/SD (Background). SNR was used to filter unreasonable data. The net fluorescence value was set as SNR <0.05 and SNR to 0.001. The net fluorescence value was calculated after subtracting the blank control. The NFI and SNR of the following unreasonable situations were set to 0.001. NFI<20 and SNR>5; SNR<0.05 and NFI>20; NFI<0.05. RLM Normalization was used to normalize the NFI and calculate the effect values of different blocks and slides. For the microarray data clustering and multivariate analysis, first a log transformation was applied, and then 'pheatmap' in the R package was used with Ward.D2 clustering to perform the cluster analysis.

c. Machine learning and Multivariate analysis of autoantigen IgM microarray data

Multivariate analysis of patient clusters based on distance metrics derived from IgM antibody levels against a panel of autoantigens. Columns with zero variation (constant values) were removed. Log-transformed scaled data showing relative differences between patients was used because the data in its raw form had different orders of magnitude, making analysis and comparison difficult. The analysis was performed using the R package "pheatmap" using the Ward.D2 clustering method and Euclidean distances.

A Random Forest classifier using the R package randomForest was fit to predict ME/CFS as the outcome on two types of data: raw and log-scaled. The purpose of this fit was to provide a rapid screen of variables for further analysis. The Variable Importance Plot for the fits was plotted. The top 10 candidates from the Log Variable Importance Plots were selected for Principal Component Analysis (PCA), a statistical methodology for dimension reduction. PCA was performed using the R packages stats (prcomp) and FactoMineR.

*4.1.14. Other statistical analysis*

All statistical calculations were performed using GraphPad Prism 10.0. Error bars displayed on graphs represent the means ± SD of three or more independent replicates of an experiment. Statistical significance was calculated separately for each experiment and is described within individual figure legends. For image analysis, three or more biological replicates per sample condition were used to generate the represented data. The results were considered significant at $P \leq 0.05$.

## CRediT authorship contribution statement

**Zheng Liu:** Formal analysis, Investigation, Methodology, Project administration, Validation, Visualization, Writing – original draft, Writing – review & editing. **Claudia Hollmann:** Investigation, Methodology. **Sharada Kalanidhi:** Data curation, Formal analysis, Methodology. **Stephanie Lamer:** Data curation, Formal analysis, Investigation. **Andreas Schlosser:** Formal analysis, Investigation, Methodology. **Emils Edgars Basens:** Formal analysis, Investigation, Methodology. **Georgy Nikolayshvili:** Investigation, Methodology. **Liba Sokolovska:** Investigation, Methodology. **Gabriela Riemekasten:** Resources. **Rebekka Rust:** Resources. **Judith Bellmann-Strobl:** Resources. **Friedemann Paul:** Resources. **Robert K. Naviaux:** Conceptualization, Methodology, Supervision. **Zaiga Nora-Krukle:** Resources. **Franziska Sotzny:** Resources. **Carmen Scheibenbogen:** Resources. **Bhupesh K. Prusty:** Conceptualization, Funding acquisition, Methodology, Supervision, Visualization, Writing – original draft, Writing – review & editing.

## Lead contact

Further information and requests for resources and reagents should be directed to Bhupesh K Prusty (bhupesh.prusty@rsu.lv).

## Ethics approval and consent to participate

The study was approved by the Ethics Committee of Charité Universitätsmedizin Berlin (EA2/067/20; EA2_066_22; EA4_174_22) in accordance with the 1964 Declaration of Helsinki and its subsequent amendments, as well as by the Medizinische Ethikkommission of JMU, Würzburg (83/23). All donors gave informed consent.

## Materials availability

This study did not generate new, unique reagents.

## Data and code availability

The mass spectrometry proteomics data for the serum immunoglobulin proteome study have been deposited in the ProteomeXchange Consortium via the PRIDE partner repository with the dataset identifier PXD065439. The raw experimental data are submitted to the Mendley database (doi: 10.17632/ph4mbrh26h.1).

Any additional information required to reanalyze the data reported in this paper is available from the lead contact upon request.

## Funding

This work was supported by grants from ME Research UK, with the financial support of the Gordon Parish Charitable Trust (to BKP), the Amar Foundation, USA (to BKP), and the Bundesministerium für Bildung und Forschung (BMBF) (grant number 01EJ2204E) (to BKP). ZL was supported by a fellowship from Bundesverband für ME/CFS - Fatigatio e.V.

## Declaration of competing interest

The authors declare that they have no known competing financial interests or personal relationships that could have appeared to influence the work reported in this paper.

## Acknowledgement

We thank the Core Unit for Confocal Microscopy and Flow Cytometry-Based Cell Sorting at the IZKF Würzburg for their support of this study. We also thank Vera Kozjak-Pavlovic (Biocenter, University of Würzburg) for sharing a custom macro for mitochondrial analysis. We appreciate AccuraScience, USA, for their assistance with mass spectrometry data analysis and Dr. Archana Prusty for her help in establishing the in-house IgG purification pipeline.

## Appendix A. Supplementary data

Supplementary data to this article can be found online at https://doi.org/10.1016/j.bbih.2026.101187.

## References

Bertinat, R., et al., 2022. Decreased NO production in endothelial cells exposed to plasma from ME/CFS patients. Vascul Pharmacol 143, 106953.

Bhatti, J.S., Bhatti, G.K., Reddy, P.H., 2017. Mitochondrial dysfunction and oxidative stress in metabolic disorders - a step towards mitochondria based therapeutic strategies. Biochim. Biophys. Acta Mol. Basis Dis. 1863, 1066–1077.

Brown, A., Jason, L.A., 2020. Meta-analysis investigating post-exertional malaise between patients and controls. J. Health Psychol. 25, 2053–2071.

Bynke, A., et al., 2020. Autoantibodies to beta-adrenergic and muscarinic cholinergic receptors in Myalgic Encephalomyelitis (ME) patients - a validation study in plasma and cerebrospinal fluid from two Swedish cohorts. Brain Behav Immun Health 7, 100107.

Chen, H.-J., et al., 2024. Transfer of IgG from long COVID patients induces symptomology in mice. bioRxiv 2024.2005.2030, 596590.

Chowdhury, S.R., et al., 2017. Chlamydia preserves the mitochondrial network necessary for replication via microRNA-dependent inhibition of fission. J. Cell Biol. 216, 1071–1089.
Cox, J., Mann, M., 2008. MaxQuant enables high peptide identification rates, individualized p.p.b.-range mass accuracies and proteome-wide protein quantification. Nat. Biotechnol. 26, 1367–1372.
Cox, J., et al., 2014. Accurate proteome-wide label-free quantification by delayed normalization and maximal peptide ratio extraction, termed MaxLFQ. Mol. Cell. Proteomics 13, 2513–2526.
Cvejic, E., Birch, R.C., Vollmer-Conna, U., 2016. Cognitive dysfunction in chronic fatigue syndrome: a review of recent evidence. Curr. Rheumatol. Rep. 18, 24.
Davis, H.E., McCorkell, L., Vogel, J.M., Topol, E.J., 2023. Long COVID: major findings, mechanisms and recommendations. Nat. Rev. Microbiol. 21, 133–146.
Donat, C., Thanei, S., Trendelenburg, M., 2019. Binding of von Willebrand Factor to Complement C1q Decreases the Phagocytosis of Cholesterol Crystals and Subsequent IL-1 Secretion in Macrophages. Front. Immunol. 10, 2712.
Esfandyarpour, R., Kashi, A., Nemat-Gorgani, M., Wilhelmy, J., Davis, R.W., 2019. A nanoelectronics-blood-based diagnostic biomarker for myalgic encephalomyelitis/chronic fatigue syndrome (ME/CFS). Proceedings of the National Academy of Sciences of the United States of America 116, 10250–10257.
Federici, A.B., 2011. The von Willebrand factor from basic mechanisms to clinical practice. Blood Transfus 9 (Suppl. 2), s1–s2.
Fluge, O., et al., 2016. Metabolic profiling indicates impaired pyruvate dehydrogenase function in myalgic encephalopathy/chronic fatigue syndrome. JCI Insight 1, e89376.
Germain, A., Levine, S.M., Hanson, M.R., 2021. In-Depth analysis of the plasma proteome in ME/CFS exposes disrupted ephrin-eph and immune System signaling. Proteomes 9.
Geyer, P.E., Holdt, L.M., Teupser, D., Mann, M., 2017. Revisiting biomarker discovery by plasma proteomics. Mol. Syst. Biol. 13, 942.
Gulve, N., et al., 2016. Anti-herpesviral effects of a novel broad range anti-microbial quaternary ammonium silane, K21. Antivir. Res. 131, 166–173.
Haffke, M., et al., 2022. Endothelial dysfunction and altered endothelial biomarkers in patients with post-COVID-19 syndrome and chronic fatigue syndrome (ME/CFS). J. Transl. Med. 20, 138.
Hartwig, J., et al., 2020. IgG stimulated β2 adrenergic receptor activation is attenuated in patients with ME/CFS. Brain, Behavior, & Immunity - Health 3, 100047.
He, J., Cheng, X., Fang, B., Shan, S., Li, Q., 2024. Mechanical stiffness promotes skin fibrosis via Piezo1-Wnt2/Wnt11-CCL24 positive feedback loop. Cell Death Dis. 15, 84.
Hennig, T., et al., 2022. Selective inhibition of miRNA processing by a herpesvirus-encoded miRNA. Nature 605, 539–544.
Herrera, J., Henke, C.A., Bitterman, P.B., 2018. Extracellular matrix as a driver of progressive fibrosis. J. Clin. Investig. 128, 45–53.
Hsieh, C.M., et al., 2000. Striated muscle preferentially expressed genes alpha and beta are two serine/threonine protein kinases derived from the same gene as the aortic preferentially expressed gene-1. J. Biol. Chem. 275, 36966–36973.
Hu, Y., et al., 2012. K-ras(G12V) transformation leads to mitochondrial dysfunction and a metabolic switch from oxidative phosphorylation to glycolysis. Cell Res. 22, 399–412.
Hughes, C.S., et al., 2019. Single-pot, solid-phase-enhanced sample preparation for proteomics experiments. Nat. Protoc. 14, 68–85.
Kadaja, L., et al., 2004. IgG from patients with liver diseases inhibit mitochondrial respiration in permeabilized oxidative muscle cells: impaired function of intracellular energetic units? Mol. Cell. Biochem. 256–257, 291–303.
Klein, R., Berg, P.A., 1990. Demonstration of "naturally occurring mitochondrial antibodies" in family members of patients with primary biliary cirrhosis. Hepatology 12, 335–341.
Lawson, N., Hsieh, C.H., March, D., Wang, X., 2016. Elevated energy production in chronic fatigue syndrome patients. J. Nat. Sci. 2.
Liu, Z., et al., 2023. Increased circulating fibronectin, depletion of natural IgM and heightened EBV, HSV-1 reactivation in ME/CFS and long COVID. medRxiv.
Loebel, M., et al., 2016. Antibodies to beta adrenergic and muscarinic cholinergic receptors in patients with Chronic Fatigue Syndrome. Brain Behav. Immun. 52, 32–39.
Luo, S., et al., 2021. SPEG binds with desmin and its deficiency causes defects in triad and focal adhesion proteins. Hum. Mol. Genet. 29, 3882–3891.
Mandarano, A.H., et al., 2020. Myalgic encephalomyelitis/chronic fatigue syndrome patients exhibit altered T cell metabolism and cytokine associations. J. Clin. Investig. 130, 1491–1505.
Marchi, S., Guilbaud, E., Tait, S.W.G., Yamazaki, T., Galluzzi, L., 2023. Mitochondrial control of inflammation. Nat. Rev. Immunol. 23, 159–173.
Martinez-Amat, A., et al., 2005. Release of alpha-actin into serum after skeletal muscle damage. Br. J. Sports Med. 39, 830–834.
Mercier-Letondal, P., Marton, C., Godet, Y., Galaine, J., 2021. Validation of a method evaluating T cell metabolic potential in compliance with ICH Q2 (R1). J. Transl. Med. 19, 21.
Milivojevic, M., et al., 2020. Plasma proteomic profiling suggests an association between antigen driven clonal B cell expansion and ME/CFS. PLoS One 15, e0236148.
Myhill, S., Booth, N.E., McLaren-Howard, J., 2009. Chronic fatigue syndrome and mitochondrial dysfunction. Int. J. Clin. Exp. Med. 2, 1–16.
Ohyama, K., et al., 2015. Proteomic profiling of antigens in circulating immune complexes associated with each of seven autoimmune diseases. Clin. Biochem. 48, 181–185.
Prusty, B.K., Chowdhury, S.R., Gulve, N., Rudel, T., 2018. Peptidase inhibitor 15 (PI15) regulates chlamydial CPAF activity. Front. Cell. Infect. Microbiol. 8, 183.
Randi, A.M., Laffan, M.A., 2017. Von Willebrand factor and angiogenesis: basic and applied issues. J Thromb Haemost 15, 13–20.
Rappsilber, J., Ishihama, Y., Mann, M., 2003. Stop and go extraction tips for matrix-assisted laser desorption/ionization, nanoelectrospray, and LC/MS sample pretreatment in proteomics. Anal. Chem. 75, 663–670.
Sandvik, M.K., et al., 2023. Endothelial dysfunction in ME/CFS patients. PLoS One 18, e0280942.
Santos Guedes de Sa, K., et al., 2024. A causal link between autoantibodies and neurological symptoms in long COVID. medRxiv.
Scheibenbogen, C., et al., 2018. Immunoadsorption to remove ss2 adrenergic receptor antibodies in Chronic Fatigue Syndrome CFS/ME. PLoS One 13, e0193672.
Schindelin, J., et al., 2012. Fiji: an open-source platform for biological-image analysis. Nat. Methods 9, 676–682.
Schreiner, P., et al., 2020. Human Herpesvirus-6 reactivation, mitochondrial fragmentation, and the coordination of antiviral and metabolic phenotypes in Myalgic Encephalomyelitis/Chronic fatigue syndrome. Immunohorizons 4, 201–215.
Shankar, V., et al., 2025. Oxidative stress is a shared characteristic of ME/CFS and long COVID. Proceedings of the National Academy of Sciences of the United States of America 122, e2426564122.
Sorokin, L., 2010. The impact of the extracellular matrix on inflammation. Nat. Rev. Immunol. 10, 712–723.
Sotzny, F., et al., 2018. Myalgic Encephalomyelitis/Chronic Fatigue Syndrome - Evidence for an autoimmune disease. Autoimmun. Rev. 17, 601–609.
Sotzny, F., et al., 2022. Dysregulated autoantibodies targeting vaso- and immunoregulatory receptors in Post COVID Syndrome correlate with symptom severity. Front. Immunol. 13, 981532.
van Campen, C., Rowe, P.C., Visser, F.C., 2023. Worsening symptoms is associated with larger cerebral blood flow abnormalities during tilt-testing in Myalgic Encephalomyelitis/Chronic fatigue syndrome (ME/CFS). Medicina (Kaunas) 59.
Vogelpoel, L.T., et al., 2014. Fc gamma receptor-TLR cross-talk elicits pro-inflammatory cytokine production by human M2 macrophages. Nat. Commun. 5, 5444.
Wang, N., Wang, X., Lan, B., Gao, Y., Cai, Y., 2025. DRP1, fission and apoptosis. Cell Death Discov. 11, 150.
Ward, B., et al., 2024. Deep plasma proteomics with data-independent acquisition: clinical Study protocol optimization with a COVID-19 cohort. J. Proteome Res. 23, 3806–3822.
Yepez, V.A., et al., 2018. OCR-Stats: robust estimation and statistical testing of mitochondrial respiration activities using Seahorse XF Analyzer. PLoS One 13, e0199938.
Zhang, H., et al., 2024. The extracellular matrix integrates mitochondrial homeostasis. Cell 187, 4289–4304 e4226.
Zhang, L., Zhou, J., Kong, W., 2025. Extracellular matrix in vascular homeostasis and disease. Nat. Rev. Cardiol. 22, 333–353.
Zinn, M.A., Jason, L.A., 2021. Cortical autonomic network connectivity predicts symptoms in myalgic encephalomyelitis/chronic fatigue syndrome (ME/CFS). Int. J. Psychophysiol. 170, 89–101.